KASDI MERBAH UNIVERSITY- OUARGLA
FACULTY OF HYDROCARBONS, RENEWABLE ENERGIES AND EARTH & UNIVERSE SCIENCES
DEPARTMENT OF EARTH AND UNIVERSE SCIENCES

Academic master's Thesis

Field: Earth and Universe Sciences

Specialty: Applied Geophysics

By

BOUTADJINE El Hadj Sebti **ATBA Abdeldjalil**

THEME

Application of inverse methods to the aero-geophysical mapping of LATEA area, Central Hoggar, southern Algeria.

Publicly defended on 10/06/2026
in front of a jury composed of:

Président :	Dr. SAHRAOUI Salah	M. A. A Univ. Ouargla
Examine :	Dr. BANSIR Fateh	M. C. B Univ. Ouargla
Supervisor :	Dr. HARROUCHI Lakhdar	M. C. A Univ. Ouargla

Academic Year: 2026/2025

Remerciements

ACKNOWLEDGEMENTS

As we reach the end of our academic journey, we **Boutadjine Elhadj Sebti** and **Atba Abd Eldjalil** would like to express our sincere gratitude to all those who supported and guided us along the way.

We are especially thankful to **Mr. Daoud Groune** for his continuous support and guidance throughout our entire internship at CRND Draria, Algiers. Your help and encouragement made a significant difference in our learning experience.

We also extend our warm thanks to **Mr. Djamel Nacer Eddine**, the director of CRND, for giving us the opportunity to complete our internship in such a professional and enriching environment.

Our deepest appreciation also goes to **Mr. Moukhtar Sid Ahmed** for his valuable support, guidance, and insights throughout our work.

Our appreciation goes as well to all the staff at **CRND** Draria—from the security personnel to every team member. Each one of you played a role in making our time there both educational and welcoming.

Finally, we express our heartfelt gratitude to **Dr. Harrouchi Lakhdar**, our supervisor, who guided us with patience and wisdom throughout the development of our graduation thesis. We also extend our thanks to **Dr. Bensir Fatah** for everything he provided us throughout our two years of study. And **Dr**. **SAHRAOUI Salah** Your support was invaluable, and we are truly thankful.

Thank you all for being part of our journey.

Dédicace

WE DEDICATE THIS MODEST WORK

TO OUR DEAR PARENTS

TO OUR BROTHERS AND SISTERS

TO ALL OUR FRIENDS AND PEERS.

H S. BOUTADJINE

Dédicace

WE DEDICATE THIS MODEST WORK
TO OUR DEAR PARENTS
TO OUR BROTHERS AND SISTERS
TO ALL OUR FRIENDS AND PEERS

A: ATBA

CONTENTS

Figures List

Tables list

ملخص

يساهم هذا البحث بشكل فعال في تعميق الفهم بالبنية تحت السطحية لمنطقة **LATEA** الواقعة ضمن كتلة الهيكلية في الهقار الأوسط **(جنوب الجزائر)** وهي منطقة تتميز بتعقيد جيولوجي كبير نظراً لتنوع وتداخل التكوينات الصخرية والبنيات التكتونية التي تنتمي إلى حقب جيولوجية مختلفة.

تركز الدراسة بشكل أساسي على تطبيق الطرق العكسية **(Inverse Methods)** على البيانات الجيوفيزيائية الجوية لتسليط الضوء على أنظمة الصدوع الرئيسية التي تميز هذه المنطقة. ويهدف البحث، من خلال اعتماد تقنيات النمذجة العكسية المتقدمة هذه، إلى التحديد الكمي والخصائص الهندسية لهذه الفوالق، بما في ذلك اتجاهاتها الجغرافية، عمق امتدادها، بالإضافة إلى كثافتها وتوزيعها الفضائي عبر مختلف أجزاء المنطقة المدروسة.

وقد أدت عمليات المعالجة والعكس الكمي للبيانات المغناطيسية الجوية إلى الكشف عن العديد من الشذوذات المغناطيسية الدالة، مما سمح برسم خرائط أكثر دقة وثنائية/ثلاثية الأبعاد لمواقع الصدوع وفهم إطارها البنيوي بشكل أوضح. تمثل النتائج المحققة مساهمة قيّمة في رسم الخرائط الجوفية للمنطقة، وتوفر محددات أساسية تساعد في إعادة بناء التاريخ الجيولوجي وتسلسل الأحداث التكتونية المعقدة التي شهدتها المنطقة.

الكلمات المفتاحية: منطقةLATEA ، الهقار الأوسط، البيانات المغناطيسية الجوية، الطرق العكسية، الخرائط البنيوية.

Abstracts

This research effectively contributes to a deeper understanding of the subsurface structure of **LATEA** the located within metacraton in central Hoggar **(southern Algeria)** a region characterized by significant geological complexity due to the diversity and intertwinement of rock formations and tectonic structures from various geological periods.

The study primarily focuses on the application of inverse methods to aero-geophysical data to highlight the major fault systems that characterize this region. By employing these advanced inversion techniques, the research aims to quantitatively evaluate and identify the geometric properties of these faults, including their geographic orientations, depth of occurrence, as well as their density and spatial distribution across different parts of the studied area.

The processing and quantitative inversion of aeromagnetic data led to the identification of several significant magnetic anomalies, which enabled a more accurate, three-dimensional delineation of fault locations and a clearer understanding of their structural framework. The achieved results represent a valuable contribution to mapping the area's subsurface architecture, providing critical constraints that assist in reconstructing its complex tectonic evolution and geological history.

Keywords: LATEA area, Central Hoggar, Aeromagnetic data, Inverse methods, Structural mapping.

Resumé

Cette recherche contribue efficacement à une compréhension plus approfondie de la structure subsurface de la région de **LATEA** située au sein du métacraton de la dans le Hoggar central **(sud de l'Algérie)** une région caractérisée par une complexité géologique majeure due à la diversité et à l'entremêlement des formations rocheuses et des structures tectoniques issues de différentes périodes géologiques.
L'étude se concentre principalement sur l'application des méthodes inverses aux données aéro-géophysiques afin de mettre en évidence les grands systèmes de failles qui caractérisent cette région. En employant ces techniques d'inversion avancées, la recherche vise à évaluer quantitativement و d'identifier les propriétés géométriques de ces failles, notamment leurs orientations géographiques, leur profondeur d'enracinement, ainsi que leur densité et leur distribution spatiale à travers les différentes parties de la zone d'étude.
Le traitement et l'inversion quantitative des données aéromagnétiques ont permis d'identifier plusieurs anomalies magnétiques significatives, ce qui a rendu possible une délinéation plus précise et tridimensionnelle de l'emplacement des failles et une meilleure compréhension de leur cadre structural. Les résultats obtenus représentent une contribution précieuse à la cartographie de l'architecture subsurface de la région, fournissant des contraintes critiques qui aident à reconstruire son évolution tectonique complexe et son histoire géologique.
Mots-clés : zone de la LATEA, Hoggar central, données aéromagnétiques, méthodes inverses, cartographie structurale.

General Introduction

Applied geophysics is one of the most prominent modern scientific tools for exploring the geological structure of the Earth's crust. It enables the study of subsurface layers without the need for direct drilling, making it a fundamental pillar in the fields of natural resource exploration and geological mapping.

This thesis focuses on the study of the **LATEA** area, located in the Central Haggar of southern Algeria a region characterized by significant geological complexity, owing to the diversity of its rock formations and the intricate interplay of tectonic structures spanning successive geological eras, from the Archean to the post-Pan-African period.

This work falls within the framework of applying inverse methods to aerogeophysical data, specifically aeromagnetic data collected as part of a comprehensive national survey conducted by the American company Aeroservice between 1969 and 1974. The study aims to identify and characterize the major fault systems cutting through the **LATEA** area by determining their geographic orientations, depths, and spatial density.

To achieve these objectives, an integrated analytical approach was adopted, encompassing the processing and interpretation of aeromagnetic data through a suite of advanced techniques, including Reduction to the Pole (RTP), energy spectrum analysis, directional derivatives, upward continuation, analytic signal, and Euler Deconvolution for estimating the depths of magnetic sources.
This thesis is organized into four main chapters:

- **Chapter I** presents the regional geological context of the Hoggar massif.
- **Chapter II** is devoted to the theoretical foundations of the geomagnetic method.
- **Chapter III** describes the characteristics of the aeromagnetic data and the processing procedures applied.
- **Chapter IV** presents and discusses the results of the quantitative interpretation of these data.

CHAPTER -I-
Geological Context

1.1. Regional Geological Context of the Hoggar

Introduction

The eastern Hoggar belongs to the Trans-Saharan Pan-African belt and is composed of adjacent terranes that were assembled during two major collisional events (Black et al., 1994). The first event corresponds to an early and intense collision with the East African Craton between 750 and 660 Ma (Liégeois et al., 1994). The second event corresponds to a later oblique collision with the West African Craton between 650 and 550 Ma.

The eastern Hoggar is located in Algeria. Covering an area of approximately 550,000 km², it constitutes the largest component of the Tuareg Shield. To the southwest, it extends into Mali through the Iforas massif, and to the south into Niger through the Aïr massif.

1.1.1. Structure of the Hoggar

The structure of the eastern Hoggar is characterized by major north–south continental-scale shear zones, particularly the 4°50′ and 8°30′ faults, which divide the region into three major structural domains. These domains differ in their structural, lithological, geochemical, and magmatic characteristics. According to Black et al. (1994), the Hoggar is considered a succession of juvenile Pan-African domains alternating with Archean and/or Eburnean rocks that were variably reworked during the Pan-African orogeny.

From east to west (Fig. 1.1), the three major domains are:

- The Eastern Hoggar
- The Central Hoggar
- The Western Hoggar

1.1.1.1. The Eastern Hoggar

The Eastern Hoggar is bounded to the west by the 8°30′ fault (Fig. 1.2). It is composed of two basement units: the Issalane block and the Djanet–Taffassasset block, separated by the Tiririne belt.

The Djanet–Taffassasset domain, which belongs to the East Saharan Craton east of the 8°30′ fault, includes a weakly metamorphosed pre-Pan-African basement and metasedimentary formations intruded by large calc-alkaline granitic batholiths (Bertrand et al., 1978).

The Tiririne Formation is a clastic unit exceeding 8,000 m in thickness. It is separated from the basement by a major unconformity corresponding to an erosional surface exposing diverse metamorphic and magmatic rocks.

• The Tiririne Belt

The Tiririne belt consists of molassic and flysch-type sediments of Upper Proterozoic age deposited unconformably on plutonic rocks dated at about 730 Ma (Caby and Andreopoulos-Renaud, 1987). It overlies unconformably the Pan-African basement of the Djanet–Taffassasset domain. The entire formation is intruded by syn- to post-tectonic granites emplaced between 600 and 580 Ma (Bertrand et al., 1978).

• The Issalane Block

The Issalane block is mainly composed of metasediments, gneisses, and migmatites. The contact between this basement of unknown age and the Tiririne series is tectonic and thrust-related.

• The Djanet–Taffassasset Block

This block is composed of volcano-sedimentary formations that underwent only weak metamorphism under greenschist facies conditions. These formations are often correlated with the Pharusian belt of the Central Hoggar and are intruded by a large syn- to late-tectonic batholith dated at approximately 725 Ma (Caby and Andreopoulos-Renaud, 1987).

1.1.1.2. The Central Hoggar

The Central Hoggar is bounded by the 4°50′ fault to the west and the 8°30′ fault to the east (Fig. 1.2). It contains very limited Neoproterozoic sedimentary and volcanic formations.

The Paleoproterozoic basement is represented by two more or less distinct metamorphic complexes separated by a doubtful unconformity (Bertrand, 1974):

• Upper Gneissic Complex

Represented by the Aleksod-type series, this complex is characterized by abundant metasedimentary rocks.

• Lower Gneissic Complex

Represented by the Arechchoum-type series, it is mainly composed of orthogneisses and rare metasediments intruded by pre- to syn-tectonic plutonic rocks

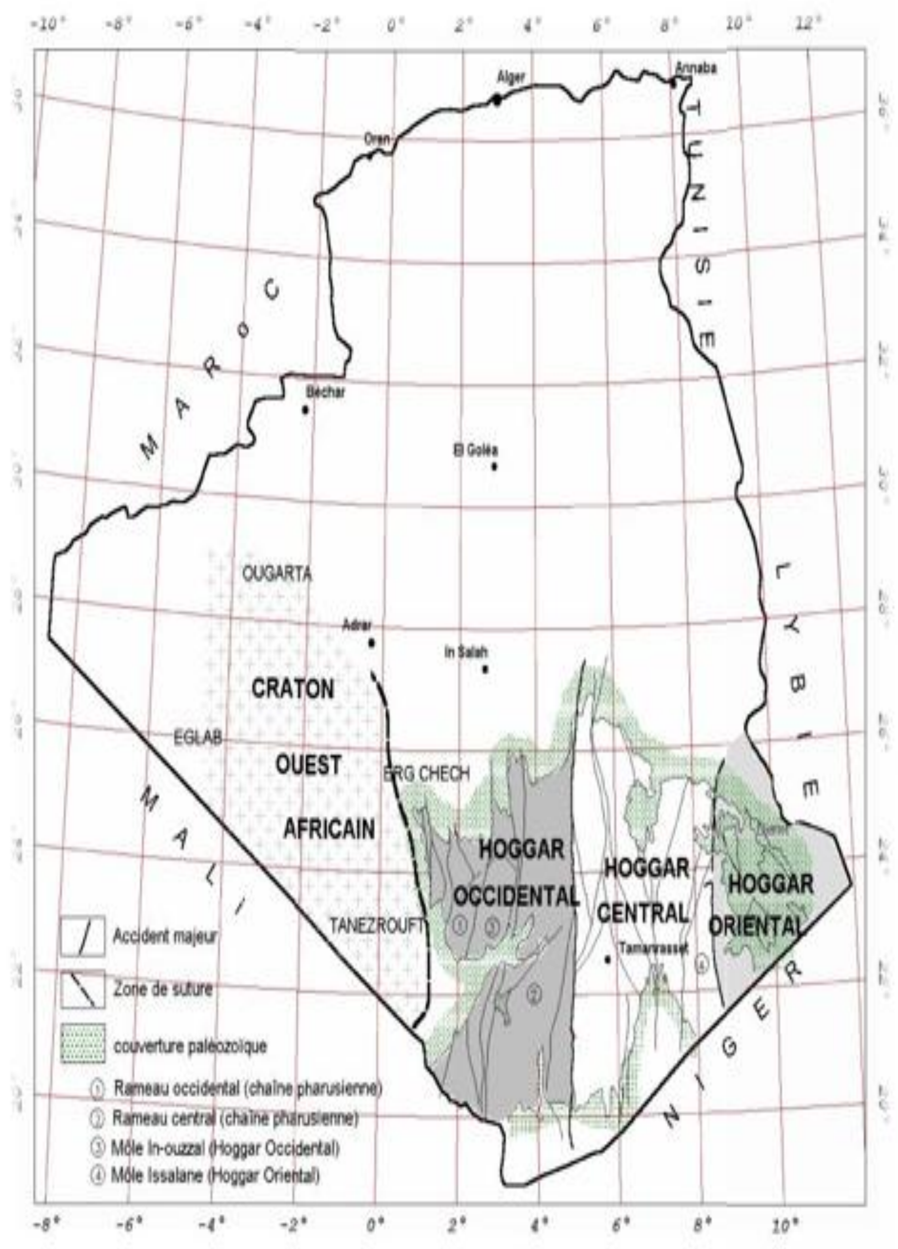

Fig. 1.1. Schematic map showing the geological domains of the Tuareg Shield (Caby et al., 2001).

1.1.1.3. The Western Hoggar

The Western Hoggar (Fig. 1.2), also called the *Pharusian Chain*, is the domain where the Pan-African orogeny is most completely represented. From the stage of oceanic opening to the stage of closure and collision between the West African Craton and the Tuareg Shield, the oceanic closure occurred through an east-dipping subduction zone, leading to an E–W collision between the passive western African margin and the active margin of the Tuareg Shield (Caby et al., 1981). In other words, from the stage of sedimentary deposition to the destruction of the chain and the accumulation of molassic deposits, the complete tectonic evolution is preserved.

The Western Hoggar is composed of two branches: the western and the eastern branches, separated by the Archean granulitic In Ouzzal massif (Fig. 2) (Allègre and Caby, 1972). The Iselfane Filonian field belongs to the eastern branch.

a. The Western Branch

It consists of three major lithostratigraphic units clearly distinguished as follows:

- **Upper Unit:** This corresponds to the Green Series (Caby, 1970). It consists essentially of flysch deposits, greywackes, tuffs, and conglomerates with intercalations of andesitic and dacitic lava flows dated at about 680 Ma.
- **Middle Unit:** This unit is mainly composed of aluminous quartzites intruded by alkaline bodies dated at approximately 750 Ma.
- **Lower Unit:** This unit is formed by two more or less distinct lithological assemblages generally separated by normal contacts, constituting the Eburnean basement known through the Tassendjanet nappe (Caby, 1970). Its platform-type sedimentary cover is generally represented by stromatolitic series.

b. The Eastern Branch

This branch is composed of two tectono-metamorphic series: Pharusian I and Pharusian II, separated by an unconformity.

- **Pharusian I Deposits:**

  The Pharusian I deposits include a volcano-sedimentary complex dominated by volcanic formations represented by the "Tiririne Series," remaining in both stratigraphic and structural unconformity over an Iburnean-age basement and intruded by syn- to late-tectonic Iburnian batholiths of Tin Tekadiouit and Taklet, dated respectively at 870 Ma and 840 Ma (Caby et al., 1982).
- **Pharusian II Deposits:**

  These are also represented by a volcano-sedimentary complex with dominant terrigenous deposits known as the "Amded-Ighellouchène Series." This series begins with a basal conglomerate unconformably overlying Pharusian I, followed by a thick detrital sequence and capped by calc-alkaline volcanism. Westward, the series laterally grades into a predominantly terrigenous sandstone-pelitic series (Gravelle, 1969).

c. The in Ouzzal Granulitic Massif

This structural unit represents an important basement nappe composed of Archean granulitic terrains. It consists essentially of a gneissic assemblage (granito-gneisses, leptynites, charnockites, and enderbites), interlayered with metasediments (quartzites and marbles) and lenses of ultrabasic rocks. Migmatization and granitization processes are very common.

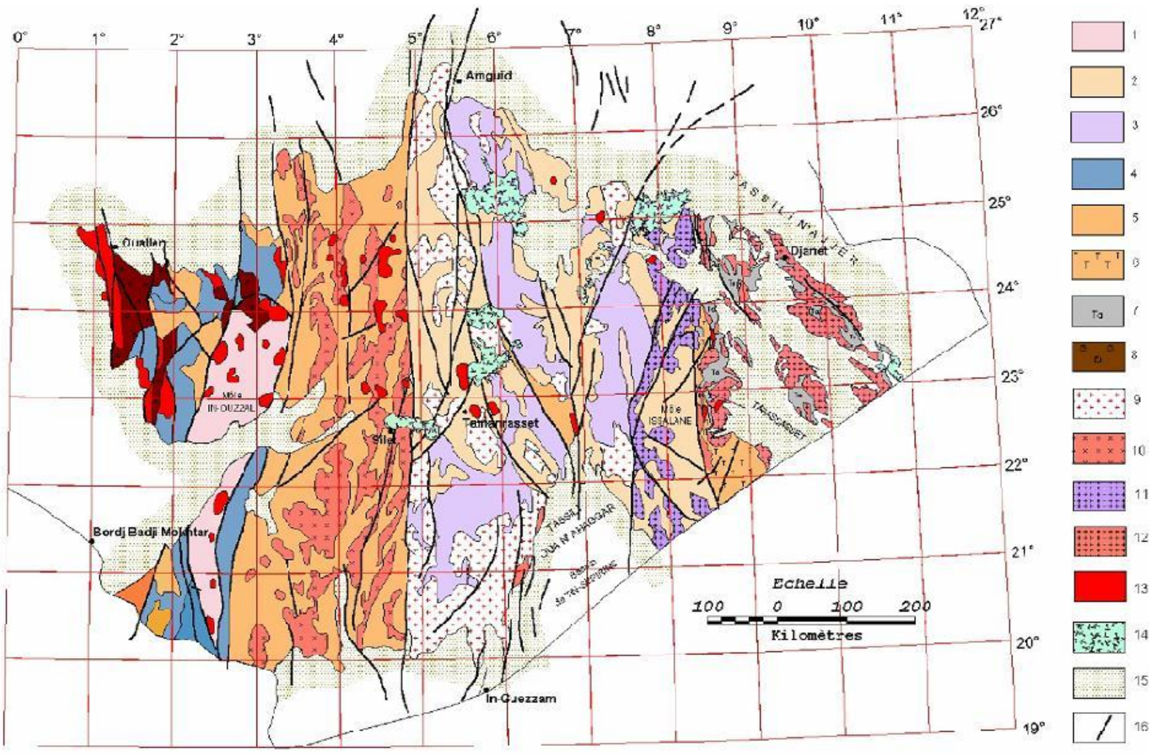

Fig. 1.2. Simplified geological map of the Hoggar (after Caby et al., 1981, modified).

1. **Archean formations.**
2. **Gneisses and metasediments of the Arrechchoum Series (Pr1).**
3. **Amphibolite-facies gneisses of the Aleksod Series (Pr2).**
4. **Undifferentiated gneisses (Pr3).**
5. **Pharusian greywackes.**
6. **Arkoses and conglomerates of the Tiririne Series (Pr4).**
7. **Volcano-sedimentary formations of Tafassasset (Pr4).**
8. **Molassic deposits (pre-platform series) of Cambrian age.**
9. **Pan-African syn-orogenic granites.**
10. **Pan-African granites.**
11. **Granites of the Eastern Hoggar.**
12. **Late Pan-African granites.**
13. **Recent basalts and volcanic rocks**
14. **Paleozoic cover.**
15 **Faults**.

1.1.2. The Terranes of the Hoggar

Studies carried out on the Hoggar massif, as well as those conducted on the Aïr massif concerning the concept of "terrane collage," led to a new subdivision of the Tuareg Shield (Black et al., 1994).

Several factors contributed to this new subdivision (Fig. 1.3), notably the difficulty and absence of correlations between the different regions of the Hoggar, as well as the incompatible characteristics observed at the level of these regions. These features can only be explained by considering large-scale tectonic displacements, hence the terminology "terranes" or "mobile terrains" (Liégeois et al., 2003).

According to this new interpretation, the Hoggar massif is considered as a juxtaposition of meridian-oriented blocks or terranes separated by regional fault zones. These terranes differ in their lithological, structural, and geochronological characteristics and are distributed within the three main compartments of the Hoggar as follows.

Table 1.1. The Different Terranes of the Hoggar

Western Hoggar	Central Hoggar	Eastern Hoggar
Timetrine (Tim)	Tilemsi (Ti)	Kidal (Ki)
Tassendjanet (Tas)	Iforas Granulitic Unit (Ug)	In Ouzzal (IO)
Ahnet (Ah)	Tirek (Ti)	In Teideni (It)
Tin Zaouatene (Za)	Iskel (Isk)	Assodé-Issalane (As-Is)
Tchilit (Tch)	Tazat (Ta)	Serouenout (Se)
Egéré-Aleksod (Eg-Al)	Azrou-n-Fad (Az)	Tefedest (Te)
Laouni (La)	Barghot (Ba)	Aouzegueur (Ao)
Edembo (Ed)	Djanet (Dj)	

Table 1.1. The Different Terranes of the Hoggar

1.1.2.1. Terranes of the Western Hoggar

The Western Hoggar is composed of eight terranes: three terranes constitute the western branch, four others form the central branch, in addition to the In Ouzzal terrane (Caby, 2003).

a. The Central Branch

- **Iskel (Isk):** Composed of sedimentary formations and sills of basic and ultrabasic rocks.
- **In Teideni (It):** Consists of detrital sediments with flysch-like characteristics and molassic deposits.
- **Tin Zaouatene (Za):** Composed of gneisses, granites, granitoids, and molasses.

- **Tirek (Ti):** Characterized by gneisses, quartzites, granitic intrusions, and Pan-African gabbros.

b. The Western Branch

- **Kidal (Ki):** Characterized by a gneissic basement.
- **Tassendjanet (Tas):** Composed of gneisses unconformably overlain by stromatolitic series.
- **Ahnet (Ah):** Characterized by quartzites and rhyolites.
- **In Ouzzal (IO):** Formed by Archean-age material structured and metamorphosed during the Eburnean event (Haddoum et al., 1994).

1.1.2.2. Terranes of the Central Hoggar

The Central Hoggar consists of six terranes separated by mylonitic corridors. These terranes are:

- **Issalane (Is):** Elongated in a north–south direction and in contact with the 8°30′ shear zone, including an ancient basement.
- **Sérouénout (Se):** Extends north–south and contains amphibolites, micaschists, and calc-alkaline granites.
- **Egéré-Aleksod (Eg-Al):** Composed of Archean and Paleoproterozoic granulitic gneisses.
- **Azrou-n-Fad (Az):** Has the same lithological composition as the Egéré-Aleksod terrane.
- **Tefedest (Te):** Includes an amphibolitic basement.
- **Laouni (La):** Distinguished by abundant post-tectonic granite intrusions.

1.1.2.3. Terranes of the Eastern Hoggar

The Eastern Hoggar consists of three terranes: Djanet (Dj), Edembo (Ed), and Aouzegueur (Ao), sharing as a common boundary the 8°30′ shear zone. These terranes are juxtaposed through NW–SE oriented fault systems.

- **Djanet (Dj):** Characterized by volcanoclastic and sedimentary rocks.
- **Edembo (Ed):** Composed of a granitic-gneissic basement, sediments, and rhyolites.
- **Aouzegueur (Ao):** Includes sediments, amphibolites, and ophiolites.

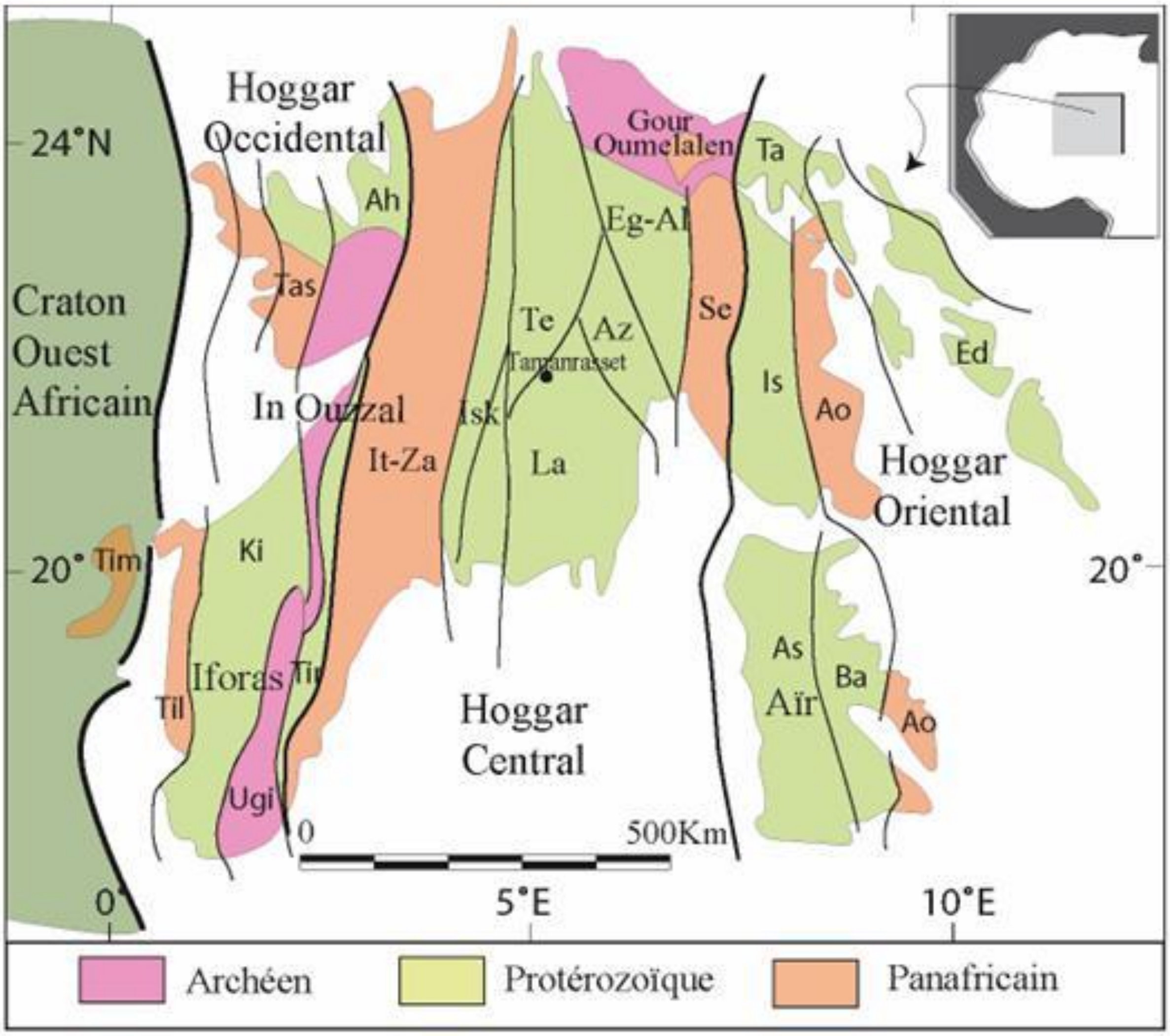

Fig. 1.3. Location map of the Hoggar and its subdivision into different terranes according to Black et al. (1994). Abbreviations: Tim = Timetrine; Til = Tilemsi; Ugi = Iforas; Ti = Tirek; Ki = Kidal; Tas = Tassendjanet; Ah = Ahnet; Isk = Iskel; La = Laouni; Te = Tefedest; Az = Azrou; Eg = Egéré-Aleksod; Se = Sérouénout; Ta = Tazat; Is = Issalane; As = Assodé; Ba = Barghot; Ao = Aouzegueur; Ed = Edembo; It-Za = In Teideni–Tin Zaouate

1.1.3. Tectono-Metamorphic Events

The principal tectono-metamorphic events defined in the Hoggar are the following:

- **The Eburnean Event (2000 ± 200 Ma):** Well defined in the In Ouzzal massif.
- **The Kibaran Event (1000 ± 100 Ma):** Defined with some uncertainty in the Aleksod region.
- **The Early Pan-African Event ("Pharusian Chain") (650–600 Ma):** Defined in the Western Hoggar.
- **The Late Pan-African Event ("Tiririnian Chain") (650–600 Ma):** Defined in the Eastern Hoggar.

1.1.4. Lithostratigraphic Formations

From a lithostratigraphic point of view, the following formations are distinguished in the Hoggar:

- **Archean formations** (>2700 Ma), represented in the In Ouzzal massif.
- **Lower Proterozoic formations** (2000–2700 Ma), represented by the Arrechchoum Series.
- **Middle Proterozoic formations** (1000–2000 Ma), represented by the Aleksod Series.
- **Upper Proterozoic formations** (800–1000 Ma), represented by stromatolitic series.
- **Terminal Proterozoic formations** (650–800 Ma).
- **Eocambrian formations** (<570 Ma), represented by the northwestern series of the Western Hoggar.

CHAPTER -II-

Geomagnetic Method

2.1 INTRODUCTION

The study of geomagnetism (terrestrial magnetism) can be considered the oldest geophysical method. It is accepted that the Earth behaves like a large, somewhat irregular magnet. Sir William Gilbert (1544–1603) conducted the first scientific research on terrestrial magnetism and showed that the magnetic field is equivalent to that of a permanent magnet placed roughly in a North-South direction, located near the Earth's rotation axis. However, it was not until 1843 that Von Wrede made the first use of field variations to locate deposits of magnetic ores.

2.2 BASIC CONCEPTS

2.2.1 Coulomb's Law

This is the fundamental law of magnetism. Unlike electric charges and masses, magnetic charges do not actually exist in reality. Coulomb assumed that the existence of magnetism is linked to the presence of what are called magnetic poles. A pole is heavy like a mass and active like a charge (charged mass). Physics has demonstrated that in nature there is no magnetic mass as an independent substance, and that magnetic properties are due to the motion of charged particles in atoms.

In a medium of magnetic permeability "μ", the force "F" acting between two poles P_1 and P_2 separated by distance "r" is given by:

$$\boldsymbol{F} = \frac{P_1 P_2}{\mu r^2} \qquad \textbf{(2.1)}$$

F = force in dynes ($cm \cdot g/s^2 = 10^{-5}$ N)

P_1 and P_2: magnetic masses or poles.

r: distance between the two poles, **μ**: permeability of the medium (**μ = 1** in vacuum and air).

2.2.2 Magnetic Potential

The potential is the work required to move a unit pole between two points in the magnetic field. The point potential is given by:

$$\boldsymbol{U} = \frac{P}{r} \qquad \textbf{(2.2)}$$

2.2.3 Relationship Between Force and Potential

Using Coulomb's law (2.1), knowing that force is the gradient of potential in the opposite direction:

$$\boldsymbol{F} = -\nabla \boldsymbol{U} = -\frac{\partial U}{\partial r} \qquad \textbf{(2.3)}$$

Magnetic induction is the sum of the external and internal field vectors; its direction is toward the magnetic North. Magnetic induction is given by:

$$\vec{B} = \mu_0 \vec{H} + \mu \vec{J} \qquad \textbf{(2.4)}$$

Where:

μ_0 = permeability of vacuum.

μ = permeability of the medium.

H = intensity of the geomagnetic field.

J = magnetization.

Unit of magnetic induction in the (SI) system: [B] = [Tesla] and in the (cgs) system: [B] = [Gauss]. Unit of measurement: in the (SI) system: [H] = [A/m] and in the (cgs) system: [H] = [Oersted].

2.2.4 Concept of the Dipole

A magnetic dipole is the combination of 2 magnetic charges of opposite sign (poles), separated by a short distance. Dipoles have a magnetic moment m, represented by a vector oriented from + (North) toward − (South). As a first approximation, the Earth's magnetic field is generated by a dipole located at the center of the Earth. This "fictitious" dipole is placed along a line making an angle of 11.5° with the rotation axis (Fig. 2.1). Such a schematic structure of the Earth's magnetic field is called the Gauss field.

The real field is irregular, and the true magnetic poles do not coincide with the geomagnetic poles and are not diametrically opposite (Table 2.1).

		Latitude	Longitude
Geomagnetic Poles	North Geomagnetic	78.5° N	111° W
Geomagnetic Poles	South Geomagnetic	78.5° S	111° W
Magnetic Poles	North Magnetic	75.5° N	101° W
Magnetic Poles	South Magnetic	67° S	143° W

Table 2.1 — Geographic location of Geomagnetic and Magnetic poles.

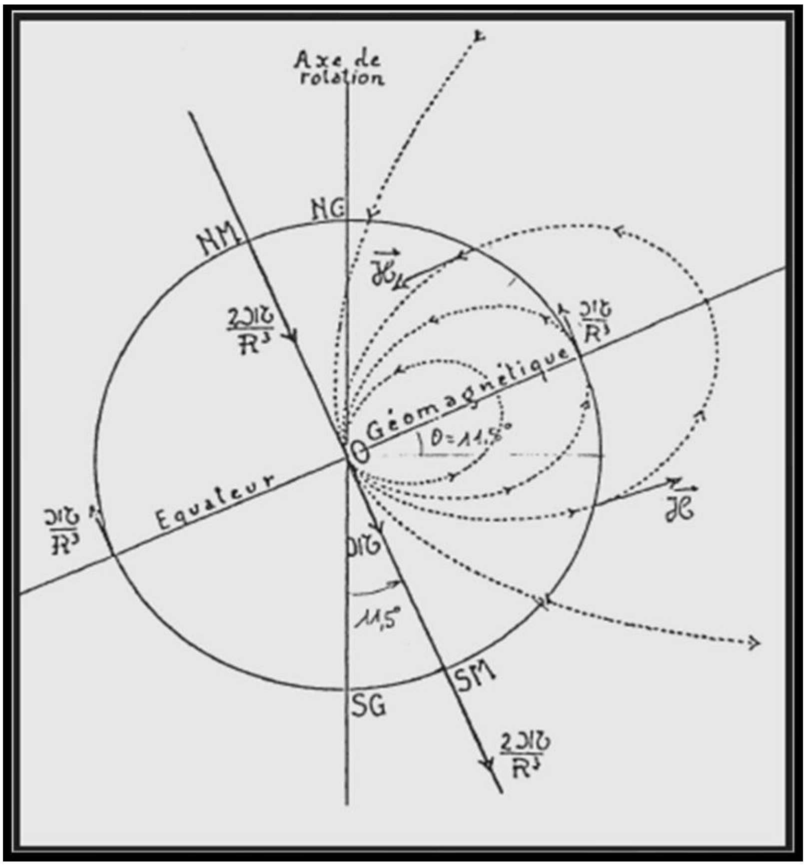

Fig. 2.1 — The Earth's magnetic field generated by a dipole at the Earth's center.

2.3 THE GEOMAGNETIC FIELD

The Earth's magnetic field, or geomagnetic field, has been the subject of numerous studies over several centuries. It is a phenomenon that varies in both space and time, characterized by its direction and intensity at every point on the Earth's surface. The geomagnetic field is the sum of two parts (Le Mouël, 1969):

The external field, produced by electrical currents flowing in the ionosphere and magnetosphere, is characterized by:

- Periodic fluctuations (daily, lunar, and annual) resulting from the distortion of the terrestrial magnetic field by solar winds.
- Rapid, weak random pulsations caused by oscillations in the ionosphere and magnetosphere.
- Disturbed days and sudden-onset magnetic storms, caused by plasma bursts emitted by the Sun, which produce polar auroras.

The internal magnetic field is the superposition of: (1) the main magnetic field, resulting from a dynamo effect at the outer core surface (~99% of the observed surface field), and (2) the crustal anomaly field, resulting from the magnetization of materials in the Earth's crust and upper mantle.

2.3.1 The International Geomagnetic Reference Field (IGRF)

International geomagnetism bodies have adopted a mathematical representation of the internal-origin field (normal field), called the IGRF. This field is determined for a given epoch and is associated with a secular variation model. The scalar potential is expanded as:

$$\boldsymbol{U(r,\theta,\varphi,t) \;=\; a\,\Sigma\Sigma\,(r/a)^{n}\,[q^{m}{}_{n}cos(m\varphi) \;+\; s^{m}{}_{n}sin(m\varphi)]\,P^{m}{}_{n}(cos\theta)}$$

$$\boldsymbol{+\,a\,\Sigma\Sigma\,\frac{a^{n+1}}{r}\;[g^{m}{}_{n}cos(m\varphi) \;+\; h^{m}{}_{n}sin(m\varphi)]\,P^{m}{}_{n}(cos\theta)} \qquad (2.5)$$

Where:

(r, θ, φ) are spherical coordinates.

t = time.

a = 6371.2 km.

n, m = degree and order.

g_n^m, h_n^m = internal Gauss coefficients.

q_n^m, s_n^m = external Gauss coefficients.

In a source-free medium: B = −grad(U) and $\nabla^2 U = 0$ (Laplace's equation).

2.3.2 Elements of the Geomagnetic Field

At every point on the Earth's surface, geomagnetic field B is represented by its intensity F as a vector; this vector changes its orientation from point to point. By convention, B is decomposed in a Cartesian or spherical coordinate system (**Telford et al., 1998; Le Mouël, 1969**).

2.3.2.1 In the Cartesian Coordinate System

The elements of the geomagnetic field in Cartesian coordinates (Fig. 2.2) are given by:

$$\boldsymbol{F^2 = H^2 + Z^2 = X^2 + Y^2 + Z^2}$$

$$\boldsymbol{H = F \cdot cos(I)} \qquad \boldsymbol{Z = F \cdot sin(I)}$$

$$\boldsymbol{X = H \cdot cos(D)} \qquad \boldsymbol{Y = H \cdot sin(D)} \qquad \textbf{(2.6)}$$

$$\boldsymbol{tan(D) = \frac{Y}{X}} \qquad \boldsymbol{tan(I) = \frac{Z}{H}}$$

The x-axis points toward geographic North, y toward East, z downward.

H is the horizontal component (compass direction).

Z the vertical component.

D (declination) is the angle between H and x.

I (inclination) is the angle between H and z.

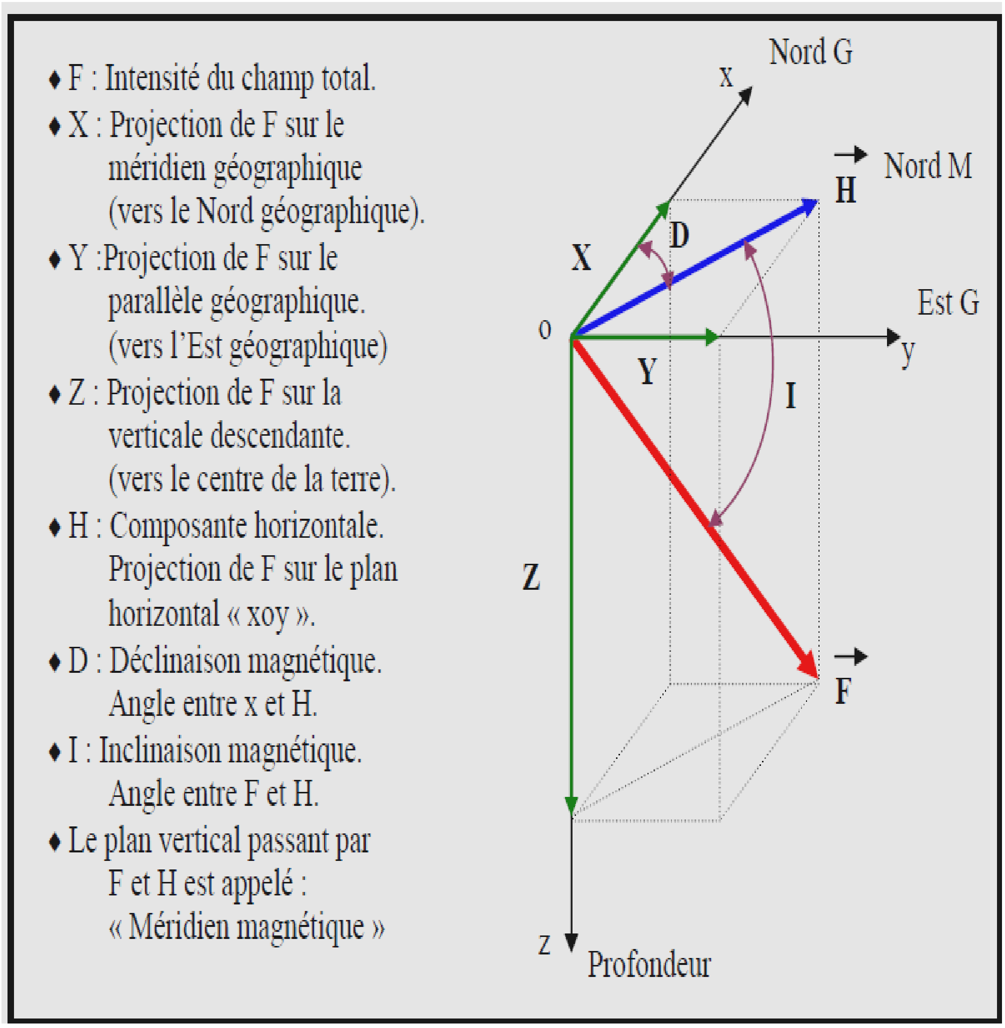

Fig. 2.2 — Elements of the geomagnetic field in the Cartesian coordinate system.

2.3.2.2 In the Spherical Coordinate System

The components of the geomagnetic field (internal sources) in spherical coordinates (Fig. 2.3):

$$B_r = -\frac{\partial U}{\partial r}$$

$$B_\theta = -\frac{1}{r} \cdot \frac{\partial U}{\partial \theta}$$

$$B_\varphi = -\frac{1}{r\,sin\theta} \cdot \frac{\partial U}{\partial \varphi}$$

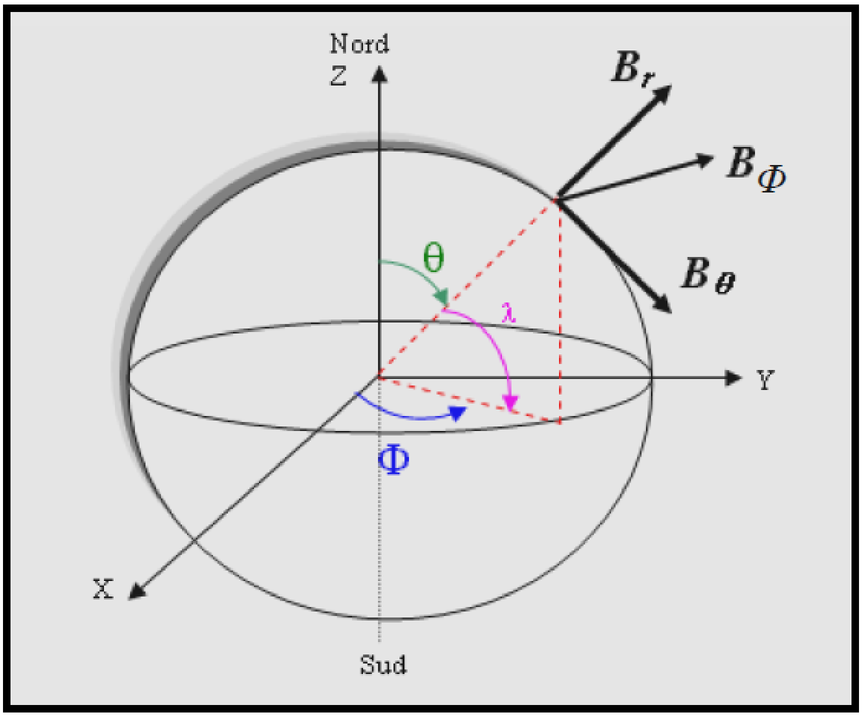

Fig. 2.3 — Elements of the geomagnetic field in the spherical coordinate system.

2.3.3 Variations of the Geomagnetic Field

During a magnetic survey, measurements taken at the same point vary as a function of time. Two types of variation are distinguished: secular (internal) and regular diurnal.

2.3.3.1 Secular Internal Variations

Long-period variations originating in the core are called secular variations. Data from the London and Paris observatories since 1540 show that inclination has varied by 10° (75° to 65°) and declination by 35° (10°E to 25°W, then back to 10°W) over this period (Fig. 2.4). Short-period variations (annual or smaller) are mainly caused by electric currents flowing in the ionosphere and the magnetosphere.

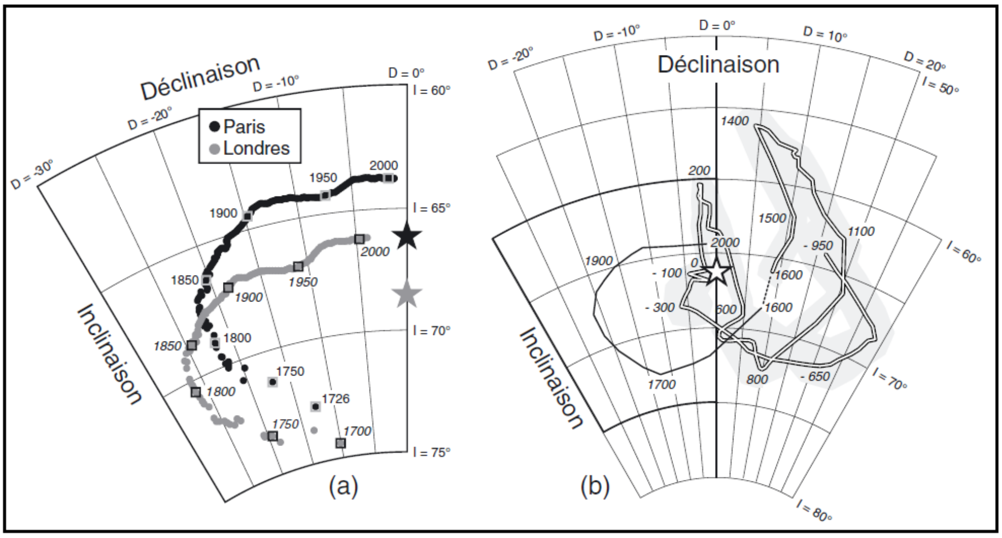

Fig. 2.4 — Secular variation of the geomagnetic field: Paris (black) and London (grey) observatories (a); archaeomagnetic data over 3 millennia (b) (Dubois 2011).

Fig.2.4 Secular variation:

evolution of the direction (Declination, Inclination) of the magnetic field (a) from 1700 to the present day, as measured in the observatories in Paris (black points) and London (gray points), and (b) determined over the last 3 millennia by archaeomagnetic studies from 950 BC (–950) to 1600 AD (black and white curve) and observatory records from 1600 to the present day (black curve), in France (Dubois 2011).

2.3.3.2 Regular Diurnal Variations

They are short periods (annual or smaller), caused essentially by electric currents circulating in the ionosphere and the magnetosphere. The diurnal variation follows the solar rhythm. Moreover, the amplitude of the variation is influenced by the activity of the sun, which reaches a maximum every 11 years.

The movement of the conducting ionosphere in the field of the permanent magnet that constitutes the Earth induces currents in the ionosphere, which produce an additional magnetic field, a field that constitutes the diurnal variation. The two sources of movements cause two cycles of variations (Giroux and Chouteau, 2011):

- ❖ A cycle that follows the solar rhythm (cycle of 24h, 11 years)
- ❖ A cycle that follows the lunar-solar tides

2.4 MEASUREMENTS OF THE GEOMAGNETIC FIELD

The first instruments used in magnetometry were modified marine compasses; these instruments provided the values of the I and D components. Other instruments were developed that allowed the measurement of the H and Z components as well as the total field component F, such as magnetic variometers.

Magnetometry equipment has truly evolved thanks to new technologies. Several types of magnetometers can be distinguished, whose principle is summarized as comparing the measured force to another known force. Three types of magnetometers can be distinguished:

❖ Flux-gate magnetometer (Accuracy = 1 nT)

❖ Nuclear precession NMR magnetometer (Accuracy = 0.1-1 nT)

❖ Optical pumping magnetometer (Accuracy = 0.01 nT)

As with gravimetry, we are going to examine the methods of measuring the geomagnetic field. One can measure the three components of the geomagnetic field (F, I, and D), and the angles D and I must be measured with a precision of 3 arcseconds. The atomic or nuclear magnetic resonance magnetometer and the Zeiss 010 A and B amagnetic theodolites make it possible to achieve such precision (one arcsecond for the theodolite and a fraction of a nanotesla for the magnetometer).

Without going into the very sophisticated details of the measurements, let us retain the principles. The measurements of D and I are carried out using the zero method on a probe (dual-saturated core sensor) whose axis is placed perpendicular to the field vector; when this zero-field position is reached, it means that the perpendicular direction is in the magnetic meridian. This direction is identified using the theodolite in relation to the known direction of a beacon that is sighted from the measurement pillar. Knowing exactly the azimuth of the pillar-beacon direction, after measuring the angle between the pillar-beacon direction and the magnetic meridian, the azimuth of the magnetic meridian is deduced. Readings are taken on the perfectly leveled horizontal circle of the theodolite. The principle of measuring inclination is identical, except that the angle of the probe axis direction with the horizontal is measured on the vertical circle of the theodolite.

2.5 DEFINITION OF THE MAGNETIC FIELD ANOMALY

The magnetic anomaly field is obtained by subtracting a regional component from the measured total field. Let $\vec{\mathbf{T}}$ be the field vector at a point and $\vec{\mathbf{F}}$ the normal (regional) field vector. The total field anomaly $\mathbf{\Delta T}$ is (Blakely 1995):

$$\Delta T = |\vec{T}| - |\vec{F}| \qquad \mathbf{(2.8)}$$

Denoting $\mathbf{\Delta}\vec{\mathbf{F}}$ as the anomalous field vector due to a perturbing source:

$$\vec{T} = \vec{F} + \Delta\vec{F} \qquad \mathbf{(2.9)}$$

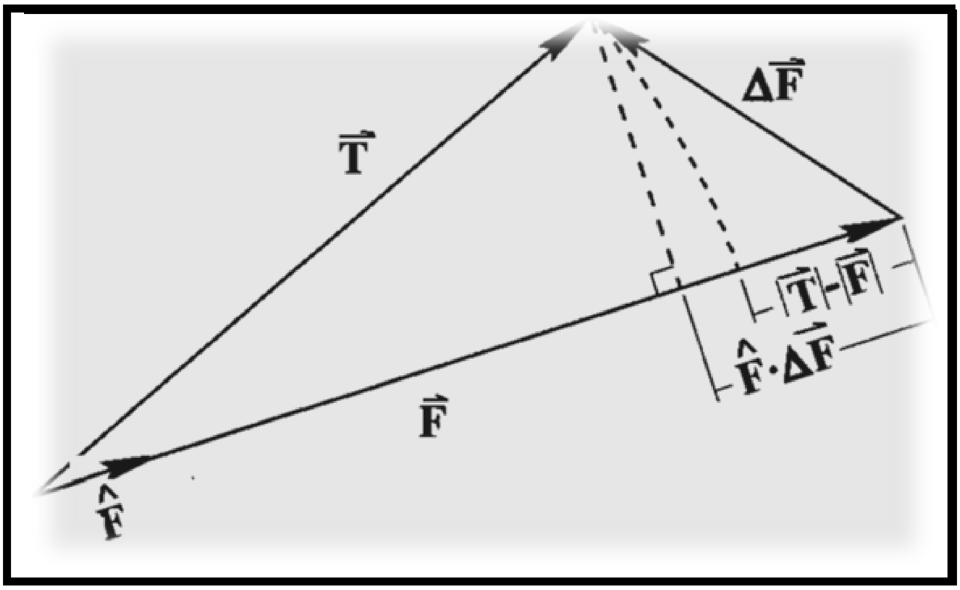

Fig. 2.5 — Vector representation of the anomalous field (Blakely 1995).

Fig. 2.5 Vector representation of the anomalous field vector. The vector T is the vector sum of the regional field F and the anomalous field $\Delta\vec{F}$, F^ with the unit vector carried by the regional field vector (Blakely 1995).

According to figure 2.5, it is clear that the anomaly of the total field does not equal the intensity of the anomalous field:

$$\Delta T =$$

To make the necessary approximations to obtain F , it is assumed

that the following hypotheses are
properly considered:

- ❖ The intensity of the anomaly field is small compared to that of the normal field (ΔF; this condition is generally met for crustal anomalies).

2.6 MAGNETIC PROPERTIES OF ROCKS

2.6.1 Magnetic Susceptibility "K"

Magnetic susceptibility K is a marker for magnetism, just as density is for gravimetry. It can be measured in situ by instruments used on outcrops or directly on samples. Magnetic susceptibility characterizes the tendency or the ability of a rock to orient itself under the influence of an ambient field. It represents the proportionality constant in the expression of the magnetization law:

$$\vec{J} = K \cdot \vec{H} \qquad (2.12)$$

Where $\vec{J}$ is the magnetization and $\vec{H}$ is the field intensity. The highest susceptibilities are found in basic igneous rocks; the lowest in sedimentary rocks (Fig. 2.6).

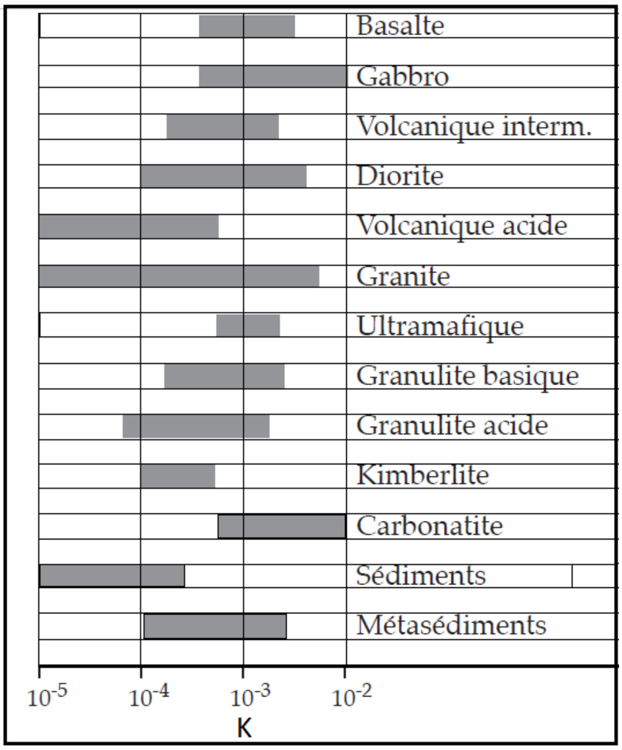

Fig. 2.6 — Magnetic susceptibilities of several rock types.

2.6.2 Magnetic Permeability μ

It is the ability of rocks to change their inductions under the effect of an external field. It represents the proportionality constant in the expression of magnetic induction B.

$$\vec{B} = \mu \vec{H} = \mu_r \mu_0 \vec{H} \qquad (2.13)$$

Where

μ is the absolute permeability

μ_r the relative permeability

μ_0 the permeability of vacuum.

The relationship between B and H is not necessarily linear. Figure 2.7 shows the hysteresis curve describing the behavior of magnetization cycles.

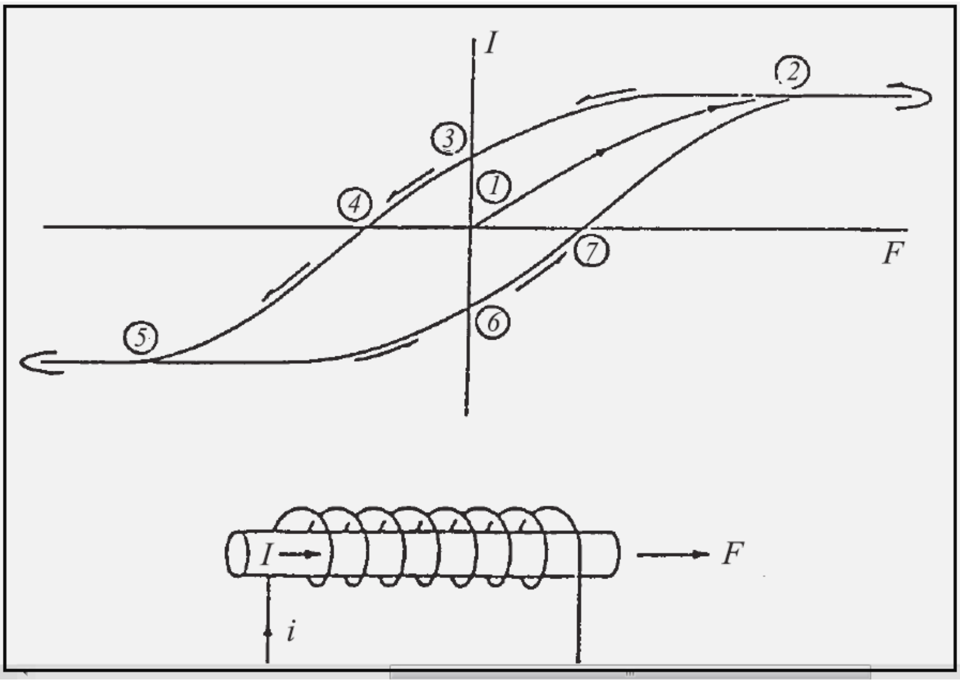

Fig. 2.7 — Hysteresis curve of a ferromagnetic substance.

Fig.2.7 Hysteresis curve showing how the magnetic moment per unit volume I in a ferromagnetic substance varies with the magnetizing field F produced by electric current in the coil. The sequence of numbers indicates the magnetization cycle.

2.6.3 Magnetic Moment

To have a density μH in the medium, it is necessary to add an additional field KH to μrH. This additional field present at a point in the occupied space is the magnetic moment M. It is expressed by the following relation (Telford et al., 1998):

$$\vec{M} = K \cdot \vec{H} \qquad (2.14)$$

2.7 MAGNETIZATION OF ROCKS

Igneous and sedimentary rocks possess a permanent (remanent) magnetic field to varying degrees. The direction of this remanent field can be completely different from the direction of the local field; it is characteristic of the local field at the time of the rock's formation. The magnetization of rocks can be defined as the magnetic moment M per unit volume v. It is due to the presence of the magnetic minerals they contain and is expressed by the following relationship:

$$\vec{m} = \nu \cdot \vec{M} \qquad (2.15)$$

The remanent magnetization of a rock is a permanent magnetization acquired by the rock called: natural remanent magnetization NRM (Natural Remanent Magnetization). In many cases, the magnetization of rocks mainly depends on the existence of an ambient magnetic field in the presence of magnetic minerals in the rock. This phenomenon is very complicated; it depends on the genesis of the rock. The main types are distinguished as follows (Chouteau, 1999):

TRM — Thermo-Remanent Magnetization

- DRM — Depositional Remanent Magnetization
- CRM — Chemical Remanent Magnetization
- IRM — Isothermal Remanent Magnetization
- VRM — Viscous Remanent Magnetization

When subjected to a magnetic field, the rocks that make up the Earth's crust are likely to acquire 2 types of magnetization:

- ❖ An induced magnetization
- ❖ A remanent magnetization.

The magnetism of materials depends on the magnetic moments of atoms or ions. According to magnetic susceptibility, three major classes are distinguished: Diamagnetism, Paramagnetism, and Ferromagnetism.

2.7.1 Diamagnetism

The body acquires a magnetization opposite to the applied field. Most solid, liquid, and gaseous bodies are diamagnetic (water, air, silica, calcite...), with weak susceptibility less than zero.

2.7.2 Paramagnetism

Concerns bodies containing iron atoms or ions. They acquire a positive magnetization in the direction of the applied field. This magnetization is weak, proportional to the applied field, decreases with temperature, and vanishes when the field is removed.

2.7.3 Ferromagnetism

For which the susceptibility K is very high and greater than zero. The magnetism in this case is due to spontaneous magnetization. This magnetization is much stronger than in the previous two cases and it continues when the surrounding field has been removed (remanence).

Any rock possessing magnetic properties contains ferromagnetic minerals (Fig.2.8), and even if they are only in trace amounts, their effect is greater than that of the host rock. A certain number Substances containing Cobalt, Nickel, Platinum, or rare earths are ferromagnetic, but natural ferromagnetics are always crystalline solids containing Iron (Iron oxides, Hematite, Magnetite, Goethite, Pyrrhotites, Pyrite).

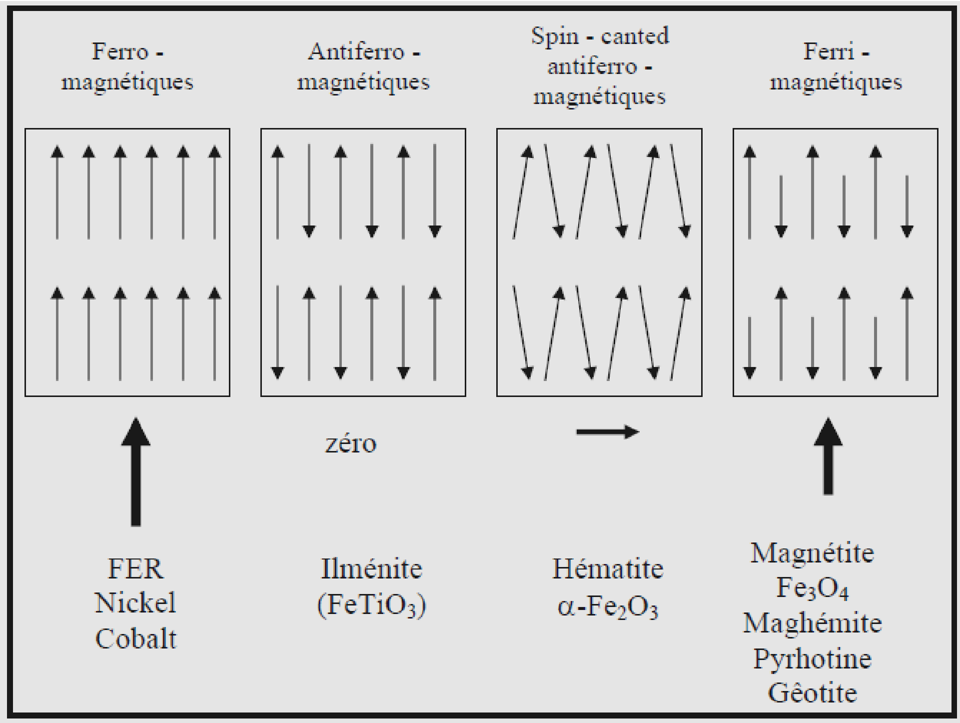

Fig. 2.8 — Classes of ferromagnetic materials.

2.8 PALEOMAGNETISM AND ARCHAEOMAGNETISM

Paleomagnetism is based on the study of the ancient magnetic field of the Earth. This discipline flourished from the 1960s onward, strongly contributing to demonstrating seafloor spreading and the formulation of plate tectonics theory.

Paleomagnetism relies on measuring the remanent magnetizations recorded by certain sedimentary or volcanic rocks. These measurements inform us about the history of the Earth's magnetic field and allow reconstruction of tectonic plate movements throughout geological history.

Within this discipline, archaeomagnetism relies on the magnetic study of archaeological materials (pottery, bricks, etc.). Rock magnetism teaches how magnetizations form and why they remain stable over very long periods. It is essential to determine the nature of the magnetic minerals and the size of the magnetic grains involved. Each rock type (volcanic, magmatic, sedimentary) acquires its magnetization through a process specific to it.

CHAPITRE III

DESCRIPTION AND PROCESSING OF AEROGEOPHYSICAL SURVEYS

3. PROCESSING AND DESCRIPTION OF AEROGEOPHYSICAL SURVEYS

3.1 DESCRIPTION OF AEROMAGNETIC DATA

3.1.1 Introduction

The aeromagnetic data made available to us are in the form of isoline maps of the total magnetic field **(Fig. 3.1b).** These maps form part of the results of an aerogeophysical survey covering the whole of Algeria and were compiled along lines of orientation perpendicular to regional geological structures between 1969 and 1974 by the American company Aeroservice **(Fig. 3.1a).** This survey was carried out with the aim of providing information on the country's regional geology and its mineral and petroleum potential **(Aeroservice, 1975).**

3.1.2 Characteristics of the régional aeromagnetic survey

This survey was conducted in two stages **(Fig. 3.1a):** the 1969 survey and the 1970–74 survey:

- **1969 Survey:** This survey covered 20% of the national territory. This was performed at a constant barometric altitude. The flight lines ran east-west over the area flown over and north-east to south-west in the southern part. The spacing between the flight lines was 5 km.
- **1970–74 survey:** this survey covered the whole of Algerian territory; this phase of the survey was carried out at a constant altitude of approximately 150 m above ground level. The flight lines were grouped into blocks that the more or less perpendicular to the direction of the main geological structures of the basement. The spacing between flight lines varied between 0.5 and 2.5 km for the lines and 50 km for the transects. The technical characteristics and results of this study are detailed below.

3.1.3 Characteristics of the aeromagnetic survey of the LATEA terranes

The aeromagnetic data for our study area and the neighboring terranes **(Fig. 3b)** were part of the results of an aerogeophysical survey covering the whole of Algeria (**Aeroservice, 1975**). These data were collected along lines of orientation perpendicular to regional geological structures between **1969** and **1974** by the Aeroservice Corporation **(Fig. 3.1a).** The flight lines ran east-west. The spacing between the lines was **2** km. The connecting lines were laid out perpendicular to the flight lines and spaced **40** km apart. The spacing between the measurement points was **46.2** m. The flight altitude was **150** m above ground level **(Aeroservice, 1975).**

3.1.4 Equipment used

The technical equipment used for the aeromagnetic survey of the **LATEA** terranes and adjacent areas is summarized in **Table 3.1** below:

Table 3.1 Techniques and equipment used for the aeromagnetic survey of LATEA and adjacent areas **(Aeroservice, 1975)**

Techniques and equipment used	Characteristics
Magnetometres	two types of magnetometres were used to measure the total magnetic field : (1) an optically pumped cesium magnétomètre with a resolution of 0.02 nT (VARIAN model) and (2) a fluxgate magnétomètre with a résolution of 0.5 nT.
Aircraft	Two types of aircraft were used to carry out the aeromagnetic survey: the Aero Commander and the Douglas DC
Altimeter	A radar altimeter was used by Aéroservice to measure the flight altitude above the ground level. This radar altimeter had an accuracy of 30 ft, and the average flight altitude was set at 150 m.
Magnetic compass	The heading of the aircraft was determined using a Sperry CL2 magnetic compass with a resolution of 1°. This was connected to the navigation system of the vehicle.
The camera	The visualization system consisted of a 35 mm continuous-film camera equipped with a numbering system to count the marks on the film at intervals of approximately 4.5 km.
The navigation system	Navigation was carried out using an ADRA-12 Doppler navigation system. The distance between lines varied from two to five kilometeres depending on the region, but averaged around two kilometeres.

Data acquisition system:	A Lancer-type data acquisition system was used to record all digital data on 1/2-inch magnetic tapes.
The graphic recorders	Two types of recorders, with two and six channels, respectively, were used for the graphical display of the magnetic and spectrometric profiles.

Table 3.1 Techniques and equipment used for the aeromagnetic survey of LATEA and adjacent areas (Aeroservice, 1975)

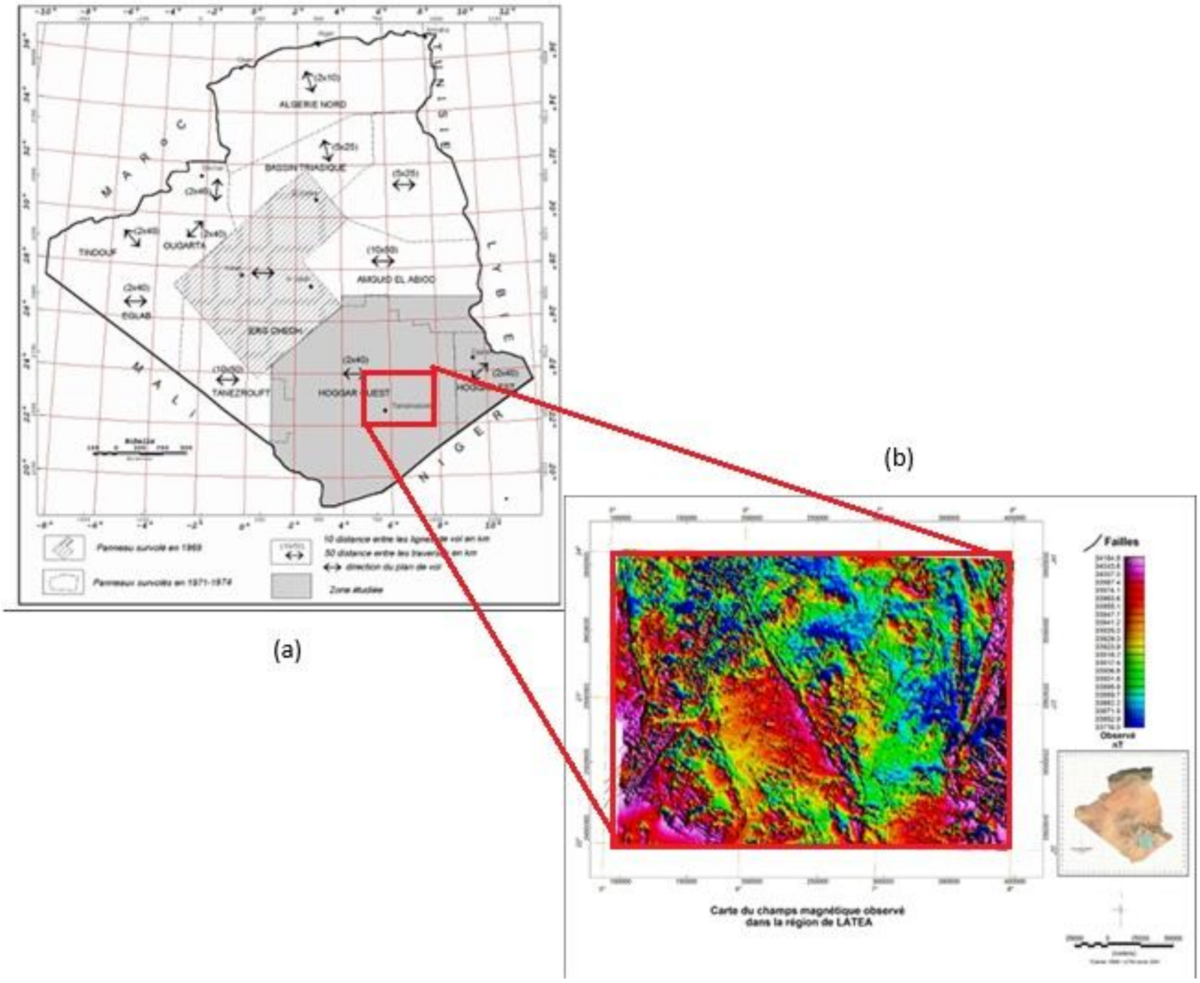

Fig. 3.1a Aeromagnetic survey covering the Algerian territory between 1969 and 1974 **(Aéroservice, 1975).** b Map of the total (raw) magnetic field from LATEA. The Cartesian coordinates (X and Y) are given in UTM Zone 31N.

3.2AEROMAGNETIC DATA PROCESSING

3.2.1 Introduction

To facilitate the interpretation of aeromagnetic data, certain mathematical processes mustbe applied to the observed measurements.

3.2.1 The anomaly field

The magnetic anomaly field was obtained by subtracting the regional component from the measured field.

Let $\vec{T}$ be the field vector at point and $\vec{F}$ be the normal or regional field vector. The total field anomaly ΔT is calculated using the following equation **(Blakely, 1995):**

$$\Delta T = \left|\vec{T}\right| - \left|\vec{F}\right| \tag{3.1}$$

If denotes $\Delta\vec{F}$ as the anomaly field vector due to a disturbing source, then the following relationship applies (Fig. 3.1):

$$\vec{T} = \vec{F} + \Delta\vec{F} \tag{3.2}$$

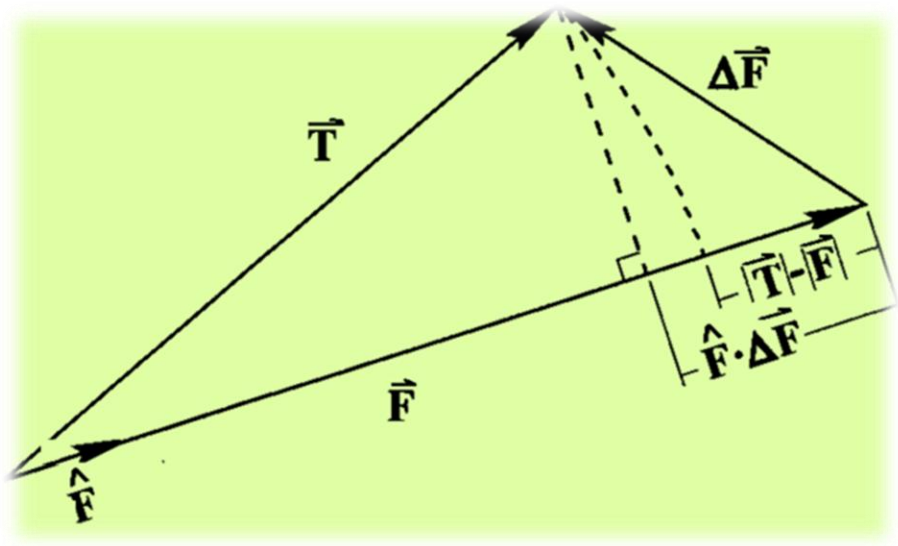

Fig. 3.2 Vector representation the anomaly Field vector. The vector $\vec{T}$ is the vector sum of the régional Field $\vec{F}$ and the anomaly Field $\Delta\vec{F}$, where $\hat{F}$ is the unit vector carried by the régional Field vector (Blakely 1995).

From Figure 3.2 it is clear that the total field anomaly is not equal to the intensity of the anomalous field.

$$\Delta T = \left|\vec{F} + \Delta\vec{F}\right| - \left|\vec{F}\right| \neq \left|\Delta\vec{F}\right| \quad \textbf{(3.3)}$$

To make the necessary approximations to obtain $\left|\Delta\vec{F}\right|$, we assume that the following hypotheses hold:

- ❖ The intensity of the anomaly field is small compared to that of the normal field $\left(\left|\vec{F}\right| \succ\succ \left|\Delta\vec{F}\right|\right)$; this condition is generally satisfied for crustal anomalies.
- ❖ The normal field vector must have an approximately fixed direction in the study domain. This is true for a space with dimensions sufficiently limited to be considered a flat surface. Therefore, the following approximation is valid

$$\Delta T = \left|\vec{F} + \Delta\vec{F}\right| - \left|\vec{F}\right| \approx \left(\vec{F}.\vec{F} + 2\vec{F}.\Delta\vec{F}\right)^{1/2} - \left|\vec{F}\right|$$

$$\approx \left(\vec{F}.\vec{F}\right)^{1/2} + (1/2)(2)\left(\vec{F}.\vec{F}\right)^{-1/2}.\left(\vec{F}.\Delta\vec{F}\right) - \left|\vec{F}\right|$$

$$= \frac{\vec{F}.\Delta\vec{F}}{\left|\vec{F}\right|}$$

$$\Delta T \approx \hat{F}.\Delta F \quad \textbf{(3.5)}$$

This relationship shows that the magnetic field anomaly is approximately represented by the projection of the anomaly field vector onto the normal field direction.

3.2.3 The local normal Field

The local normal Field of the anomalies can be represented by a polynomial of a certion degree. In the case of a bounded domain, an approximation of the normal field intensity can take the following form (Le Mouël, 1969):

$$F = \sum_{ij} a_{ij} X^i Y^j \quad (3.6)$$

Where a_{ij} *s* corresponds to the coefficients of the algebraic polynomial that must be determined. X and Y correspond to the coordinates of the points on the plane. Using Gauss's theorem, it can be shown that the field anomaly $\Delta\vec{F}$ created by a crustal structure of finite dimensions satisfies the following relationship:

$$\int_s \Delta F(X \cdot Y) dXdY = 0 \qquad (3.7)$$

This can also be written in the discrete case in the following:

$$\sum_{ij} \Delta F^{ij} = 0 \qquad (3.8)$$

This implies that the field anomalies have a mathematical expectation of zero (this property may be restricted to a limited domain), and therefore allows us to use the least squares method to determine the coefficients a_{ij} . The choice of the degree of the calculation polynomial depends on the dimensions of the study area. To estimate an appropriate reference level, we calculated a regional pseudo-field corresponding to a first-degree polynomial, which takes the following form: $F(X,Y) = a + bX + cY$. The coefficients of the first-degree polynomial are presented in Table 3.2 :

a	34076.14 nT
b	0.04817900 nT/km
c	- 0.04721973nT/km

Table 3.2 Estimation of the coefficients of the degree 1 polynomial

3.2.4 Creation of the reduced-to-the-pole magnetic anomaly map

To reposition magnetic anomalies directly above the sources that cause them, Baranov (1957) as well as Baranov and Naudy (1964) introduced a transformation known as "reduction to the pole," consisting of calculating pseudo-anomalies that would be observed in the polar magnetic region. The pseudo-anomaly map is called the reduced-to-the-pole map. Bhattacharrya (1965) performed calculations for the reduction-to-the-pole filter using a double Fourier series. Later, this technique was improved and simplified by introducing the fast Fourier transform (FFT). Reduction to the pole is an operation that consists of transforming observed anomalies into those reduced to the pole at a given location in other words, these new anomalies are those that would be observed if the field were vertical in the study area. This simplifies the interpretation of magnetic field data. The Fourier transform of the reduction-to-the-pole formula represents a special case of induced magnetization (Gunn, 1975). It is necessary to calculate the reduction to the pole to bring the anomalies directly above the geological structures that generate them, since any analysis of anomalies is somewhat affected by both the inclination of the magnetic field and the direction of magnetization of the sources, the reduction to the magnetic pole transforms the magnetic map into one that would be obtained at the magnetic pole.

Before applying this transformation, the valuers of the componetes of the geomagnetic field in the area under study must be known . In this case, the reduced-to-the-pole magnetic anomaly map was produced with an inclination (I=…..) and declination (D=…..°W) at the central point of the study area, determined using the IGRF 1965 model.

Geomagnetic field	F=36700 nT
Declination	D=27°
Inclination	I=4.7°W

Table 3.2 Elements of the geomagnetic field in the area under study

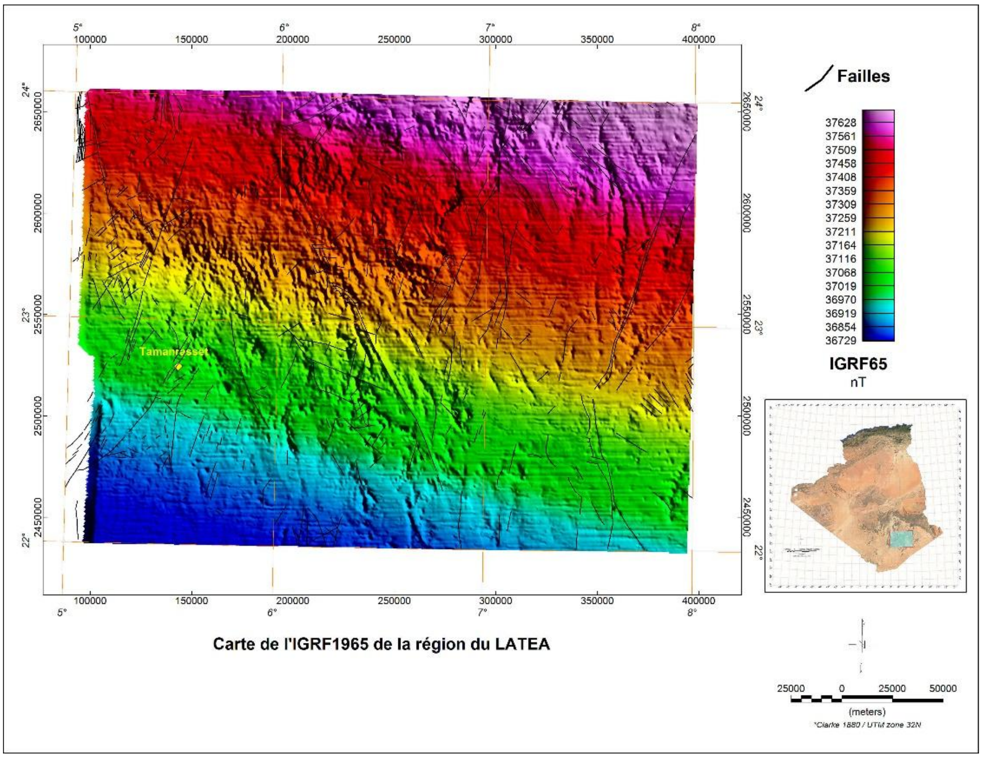

Carte de l'IGRF1965 de la région du LATEA

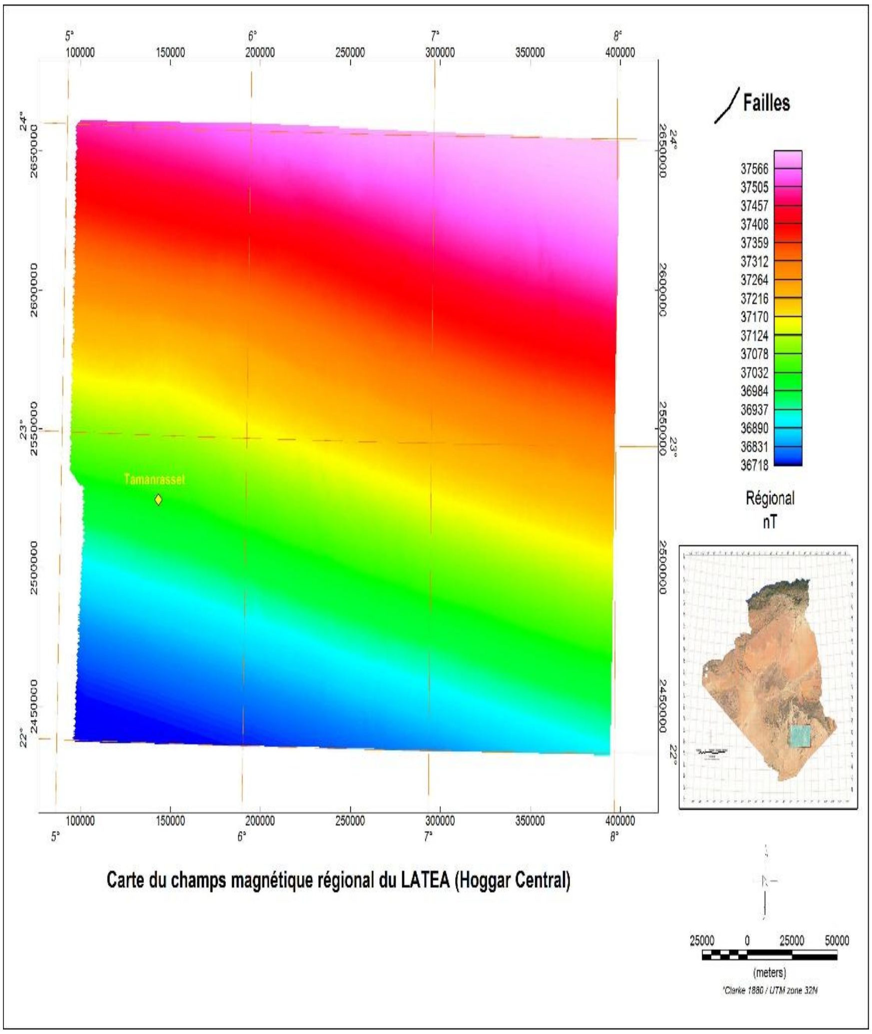

Fig. 3.3 a IGRF65 map of LATEA. B. Map of the régional Magnetic Field of LATEA (Central Hoggar)

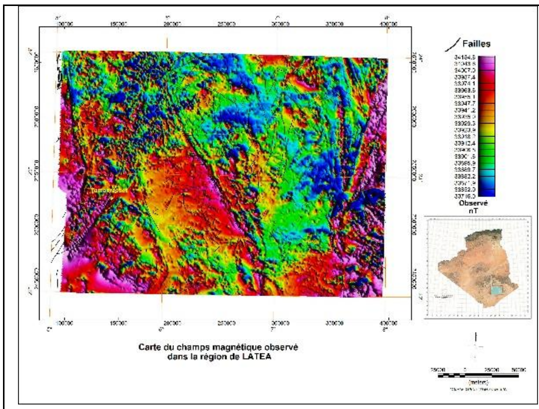

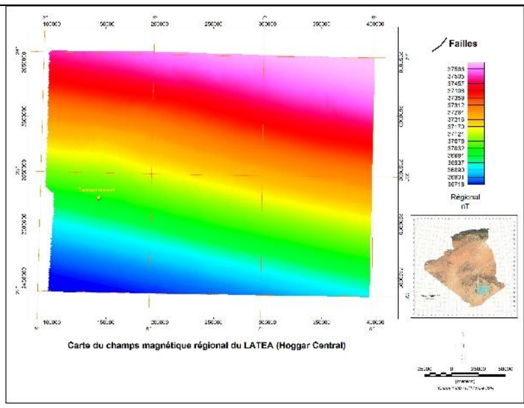

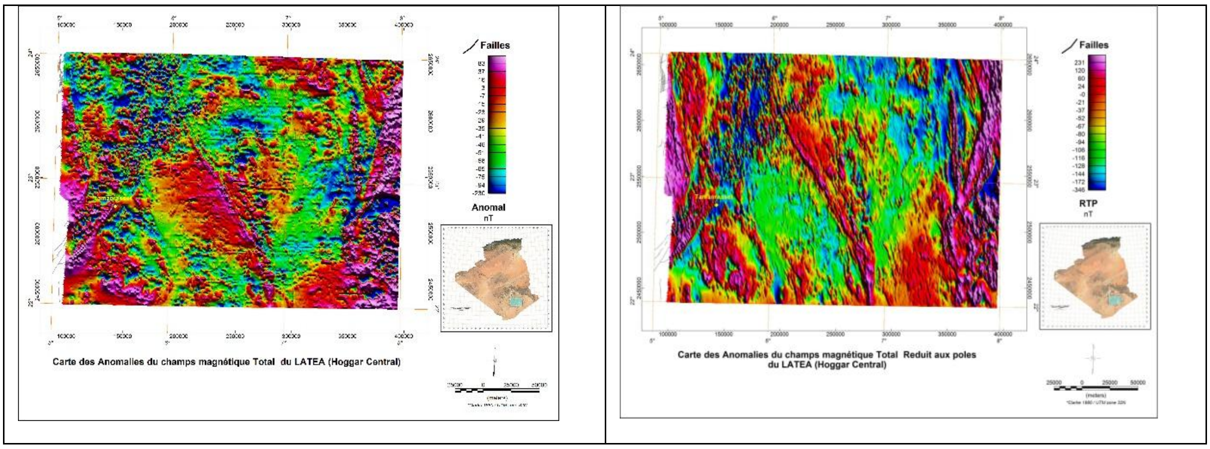

Fig.3.4a Map of the total magnetic field of LATEA, b Map of the normal (regional) magnetic field of the study area. c Map of residual magnetic anomalies. d Map of magnetic anomalies reduced at the poles. The Cartesian coordinates (X and Y) are given in UTM Zone 31N.

CHAPTER -IV-
Interpretation of aeromagnetic data

4.1. Pole Reduction (RTP)

Unlike the gravitational field, which is vertical and always directed downward, both the magnetization vector and the inducing magnetic field vector are generally inclined, resulting in asymmetric magnetic anomalies. This effect is not observed near the magnetic poles, where the geomagnetic field is vertical and behaves similarly to the gravity field.

To reposition magnetic anomalies directly above their causative sources, Baranov (1957), followed by Baranov and Naudy (1964), introduced a transformation known as *reduction to the pole* (RTP). This transformation consists of calculating pseudo-anomalies that would be observed at the magnetic pole, where both the magnetization vector and the inducing magnetic field vector are vertical. The resulting map is referred to as the *reduced-to-pole map*.

For the computation of the RTP operator, the magnetic inclination (Im) and magnetic declination (Dm) values corresponding to the center of the map for the year 1972 were used, assuming a flight altitude of 150 m and considering these parameters to be constant across the study area.

Figure 4.1 presents the reduced-to-pole magnetic anomaly map of the LATEA. Positive anomalies appear slightly shifted northward, while dipolar anomalies are transformed into monopolar anomalies. The reduced-to-pole map clearly highlights the different geological structures, particularly faults and lithological contacts.

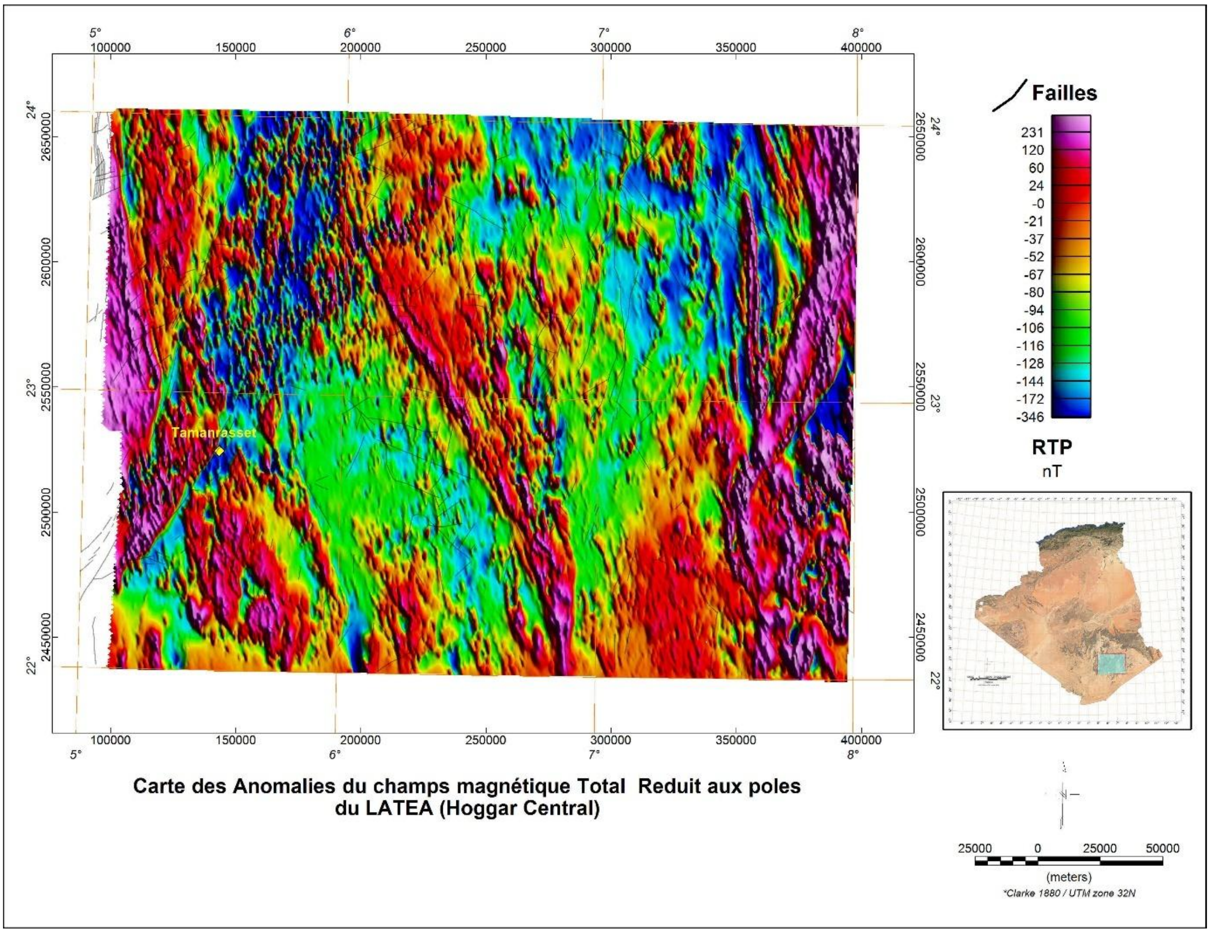

Fig 4.1 Reduced-to-pole map of the residual anomalies of the LATE

4.2 The spectrum energy

The analysis of the ES (Fig. 4.2) enables the identification of three cutoff frequencies associated with the change in slope of the spectrum. It is, therefore, possible to classify the gravity anomalies in our study area into three distinct categories (Table 4.1). The first category includes short wavelength anomalies (0.77 km < Z < 3.2 km), the second is composed of medium wavelength anomalies (3.2 km < Z < 10.87 km), and the last regroups the long wavelengths (Z > 10.87 km).

Classification	Depth (Z) km
Short wavelength	0.77 km < Z < 3.2 km
Medium wavelength	3.2 km < Z < 10.87 km
Long wavelength	Z > 10.87 km

Table 4.1 - Analysis of the LATEA aeromagnetic data ES.

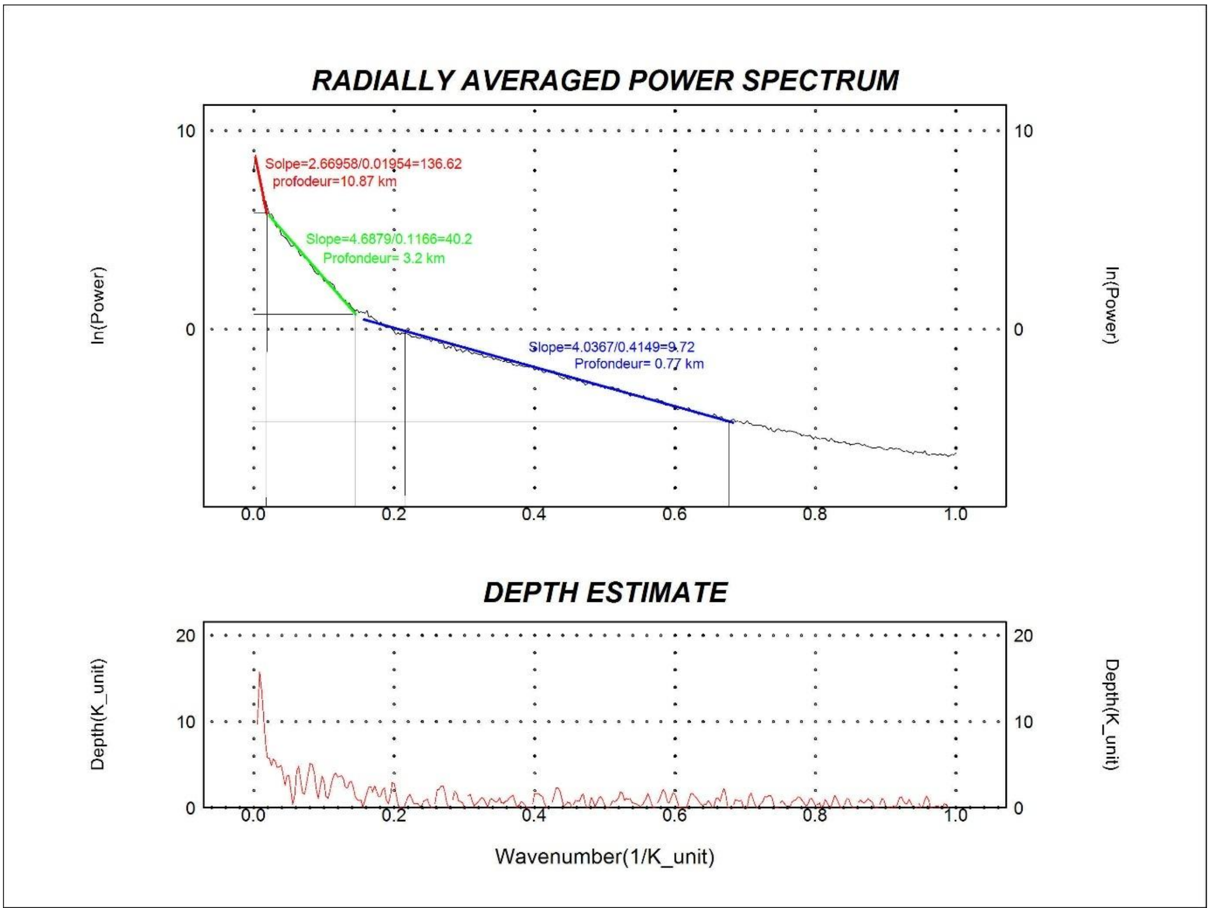

Fig.4.2 The analysis of the ES

4.3 Derivative Filters

Derivative filters enhance the effect of shallow sources while attenuating the influence of deeper ones. They emphasize magnetic anomalies and allow a better delineation of geological structures and body boundaries.

- **Horizontal derivative X:**

This filter highlights lithological contacts, geological structures, and tectonic discontinuities in the direction perpendicular to the X-axis. Figure 4.3a shows a clear differentiation in the intensity of the magnetic anomalies characterizing the various lithological and structural domains, particularly along tectonic faults.

- **Horizontal derivative Y:**

In contrast to the X-derivative, the horizontal gradient along the Y-direction enhances E–W-oriented contacts and faults. In the present case, the Y-derivative map (Fig. 4.3b) provides limited geological information, since most lithological formations and tectonic structures are generally oriented along the meridional direction. However, a SW–NE-oriented fault is clearly identified in the central part of the study area.

- **Vertical derivative Z:**

The vertical derivative (Fig. 4.3c) is used to enhance short-wavelength anomalies and emphasize the effects of shallow sources. A concentration of short-wavelength anomalies is observed in the eastern and western parts of the study area. These anomalies are probably related to shallow sources arranged in N–S and NE–SW alignments. Magnetic anomalies associated with tectonic faults, as well as lithological and structural contacts, are clearly highlighted.

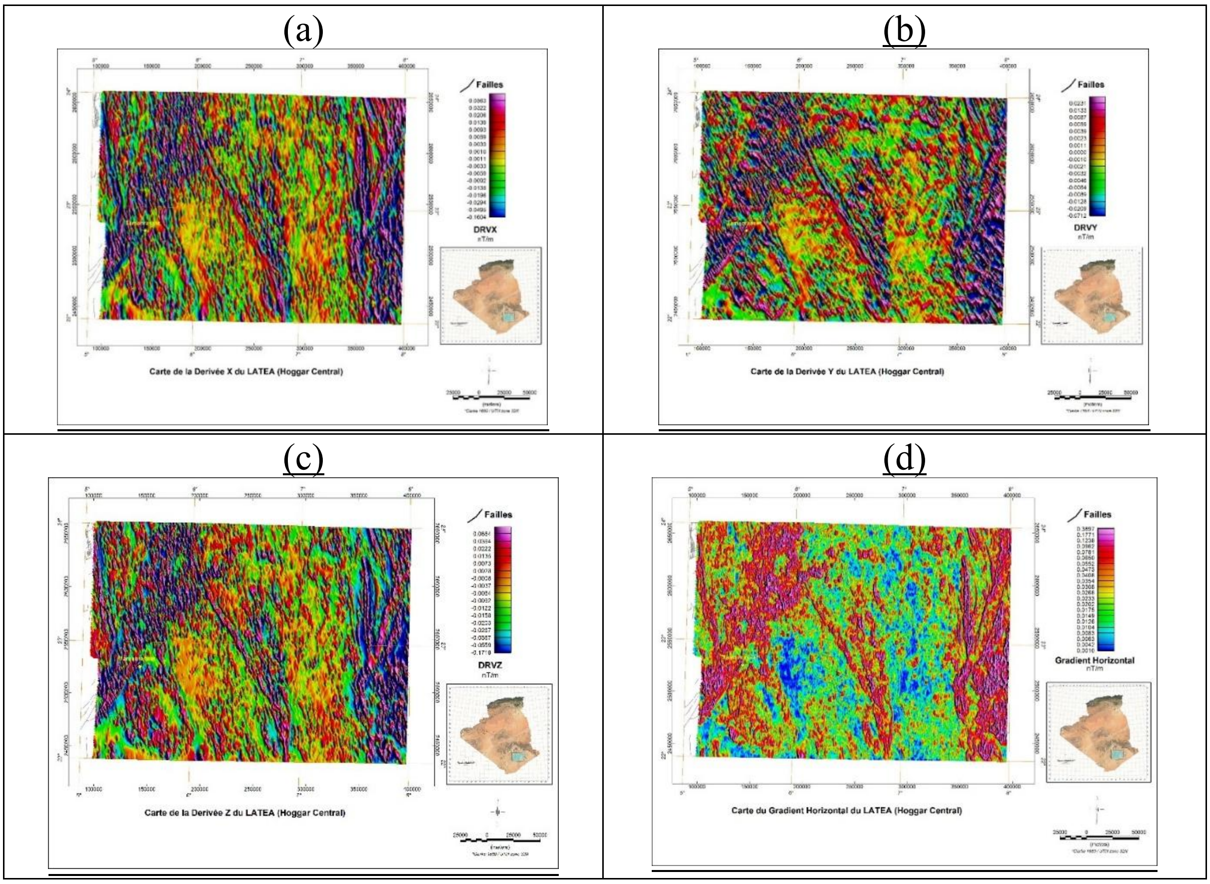

Fig.4.3 Filter derivative, a) Map of the derivative in the X-direction. b) Map of the derivative in the Y-direction. c) Map of the derivative in the Z-direction. d) Horizontal gradient map.

4.4 Upward Continuation of Aeromagnetic Data

This operation constitutes a stable and reliable filtering technique that is particularly suitable for smoothing and separating regional and residual anomalies (Jacobsen, 1987). To smooth the data and enhance the effects of deep sources, the reduced-to-pole magnetic data were upward continued to several altitudes above the observation surface. The corresponding maps are presented in **Figures 4.4a–b.**

Figure 4.4a shows the reduced-to-pole map upward continued to 3 km above the observation level (twice the grid spacing). Comparison of this map highlights the smoothing effect, which attenuates or suppresses short-wavelength anomalies in favor of longer-wavelength anomalies.

The map upward continued to 10 km exhibits a more pronounced smoothing effect **(Fig. 4.4b).** In this map, most anomalies associated with shallow sources (outcropping structures and near-surface tectonic features) are significantly attenuated, allowing anomalies generated by deeper structures to become more prominent.

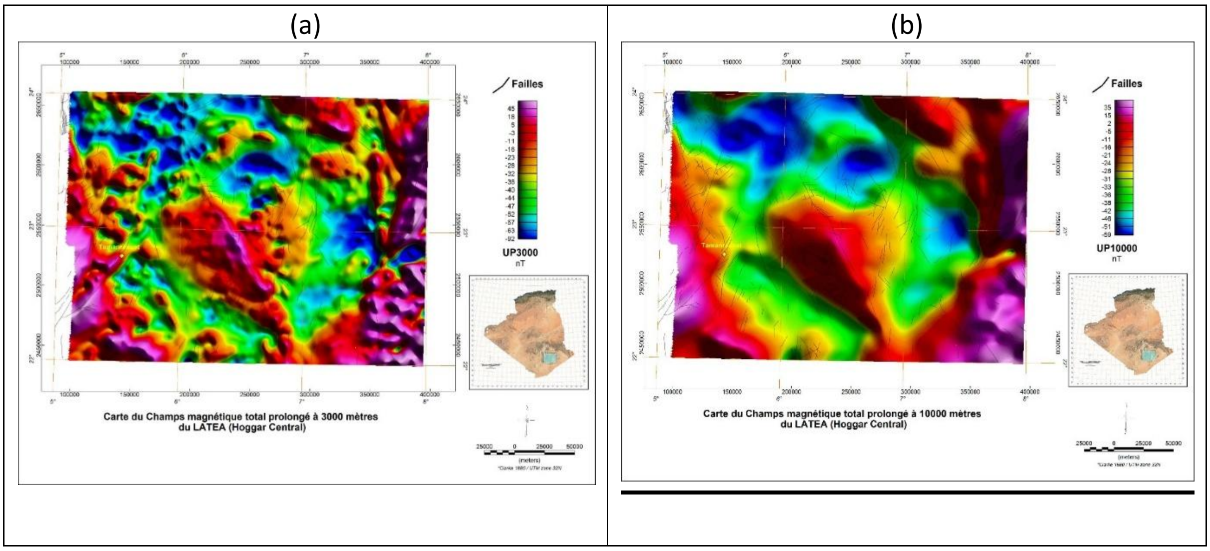

Fig.4.4 Upward Continuation of Aeromagnetic Data, a) the reduced-to-pole (RTP) map upward continued to 3 km. the RTP map upward continued to 10 km

4.2 The Analytic signal

The analytical signal technique was first introduced by Nabighian (1972, 1974, 1984), who suggested using the amplitude of the analytical signal—derived from magnetic field profiles—to determine both the depth and the location of magnetic sources. Nabighian defined the analytical signal as a "complex field derived from a complex potential," where the real and imaginary parts correspond to the horizontal and vertical derivatives of the magnetic anomaly, respectively. (Groune, 2009).

The analytical signal associated with a real-valued function defined in space is determined by the function, where "TH" represents the Hilbert transform operator (Gasquet and Witomski, 1995). In three-dimensional space, the analytical signal of a magnetic anomaly is expressed as (Nabighian, 1984; Roest et al., 1992):

$$A(x, y, z) = \frac{\partial M}{\partial x} + \frac{\partial M}{\partial y} + \frac{\partial M}{\partial z}$$

Here, represent unit vectors along the waves,ox, oy, and oz axes, respectively. The amplitude of the analytical signal is then given by:

$$|A(x,y,z)| = \sqrt{(\frac{\partial M}{\partial x})^2 + (\frac{\partial M}{\partial y})^2 + (\frac{\partial M}{\partial z})^2}$$

In the Fourier domain, this relation becomes (Roest et al., 1992):

$$\vec{t}.TF[A(x,y,z)] = \vec{h}.\nabla TF(M) + i\vec{z}.\nabla TF(M)$$

Where:

- $\vec{h} = \vec{x} + \vec{y}$: **Horizontal unit vector**.
- $\vec{t} = \vec{x} + \vec{y} + \vec{z}$: **Resultant unit vector**.
- $\nabla = ikx\vec{x} + iky\vec{y} + |k|\vec{z}$: **Opérateur du gradient dans le domaine fréquentiel – Gradient operator in the frequency domain**.
- $k = (kx, ky)$: **Wavenumber**.

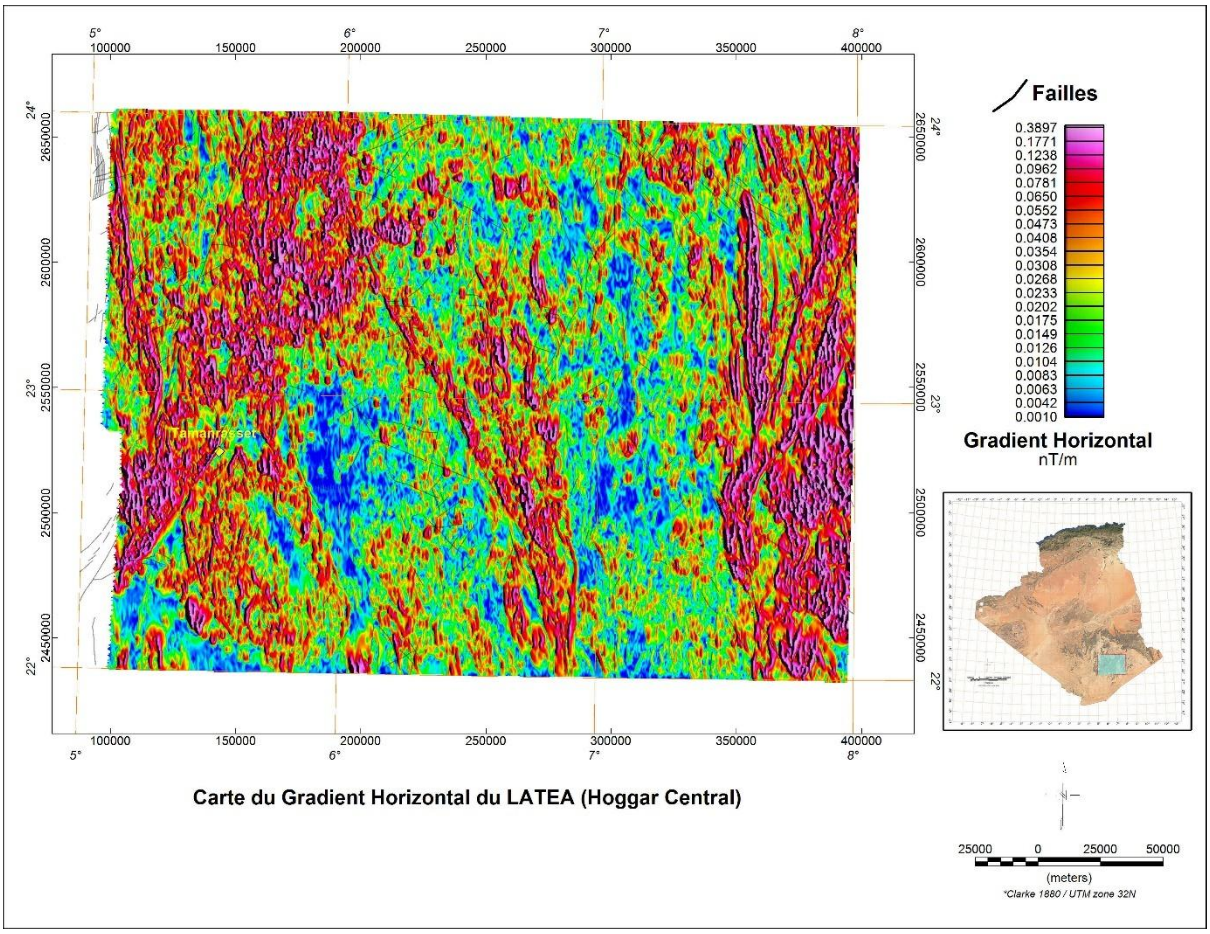

Fig 4.5 Map of the horizontal gradient of LATEA in the Central Hoggar

4.4 Euler deconvolution

The Euler deconvolution method was first introduced by Thompson (1982). It is based on Euler's homogeneity equation, which allows for the localization of sources and

estimation of their depths using magnetic profiles (2D data). Later, the technique was extended for the interpretation of gridded data (Reid et al., 1990). Since then, Euler deconvolution has undergone several improvements (Keating, 1998; Barboza et al., 1999; Mushayandebvu et al., 2001; Silva et al., 2001; Silva & Barbosa, 2003), enhancing its effectiveness in solving various geophysical problems, particularly in the identification of lineaments, geological contacts, and fault (Allek,2005).
The analytical expression of potential field anomalies (magnetic or gravity) is a function that satisfies Euler's homogeneity condition. According to this condition, a function f(x, y, z) is said to be homogeneous of degree n if it satisfies the following equation:

$$f(tx, ty, tz) = t^n f(x, y, z)$$

The type of function that frequently arises in potential theory for simple geometric shapes is typically expressed in the following form:

$$f(x, y, z) = \frac{G}{r^N}$$

Where $r = \sqrt{(x^2 + y^2 + z^2)}$ and G Independent of x, y, and z.

Value N represents the rate of variation of the field f(x, y, z) as a function of the distance between the measurement point and the source. For example, the magnetic anomaly produced by a sphere decreases proportionally to $1/r^3$, while that of an infinitely deep vertical cylinder decreases as $1/r^2$. Based on this principle, Thompson (1982) assigned a specific N value to each simple geometric model, known as the structural index in magnetics, the structural index can range between 0 and 3 depending on the shape of the source: 0 for a contact, 1 for a dyke, 2 for a vertical cylinder, and 3 for a sphere. However, real geological structures are often highly complex and do not conform exactly to simple geometric shapes. As a result, it is common in practice to choose a non-integer value for the structural index N, which typically yields more accurate results (Allek,2005).
In practical applications, the main objective is to determine the position of the sources responsible for the observed anomalies. If a source is located at the coordinates (x_0, y_0, z_0), the intensity of the magnetic field T observed at a point (x, y, z) will depend on the distance between this observation point and the source. Euler's equation, as formulated by Reid et al. (1990), is then written in the following form:

$$(x - x_0)\frac{\partial T}{\partial x} + (y - y_0)\frac{\partial T}{\partial y} + (z - z_0)\frac{\partial T}{\partial z} = -N(T - B)$$

B represents the regional component of the magnetic field, while N characterizes the structural index that best describes the anomaly. To solve this equation with four unknowns—x_0, y_0, z_0, and B—it is generally sufficient to establish a system of at least four equations. In other words, four measurements should be enough to determine the location of the magnetic source. The solution of this system of equations forms the basis of Euler deconvolution.

The classical Euler method offers a rigid and integral approach to source detection. The localization test is systematically performed for all positions of a fixed-size moving window as it scans the grid. As a result, the concepts of anomalies and their sizes are essentially disregarded. Therefore, it became

necessary to develop a localization method using Euler's technique that targets only those windows likely to contain an anomaly, while dynamically adapting the window size to match the dimensions of each detected anomaly.

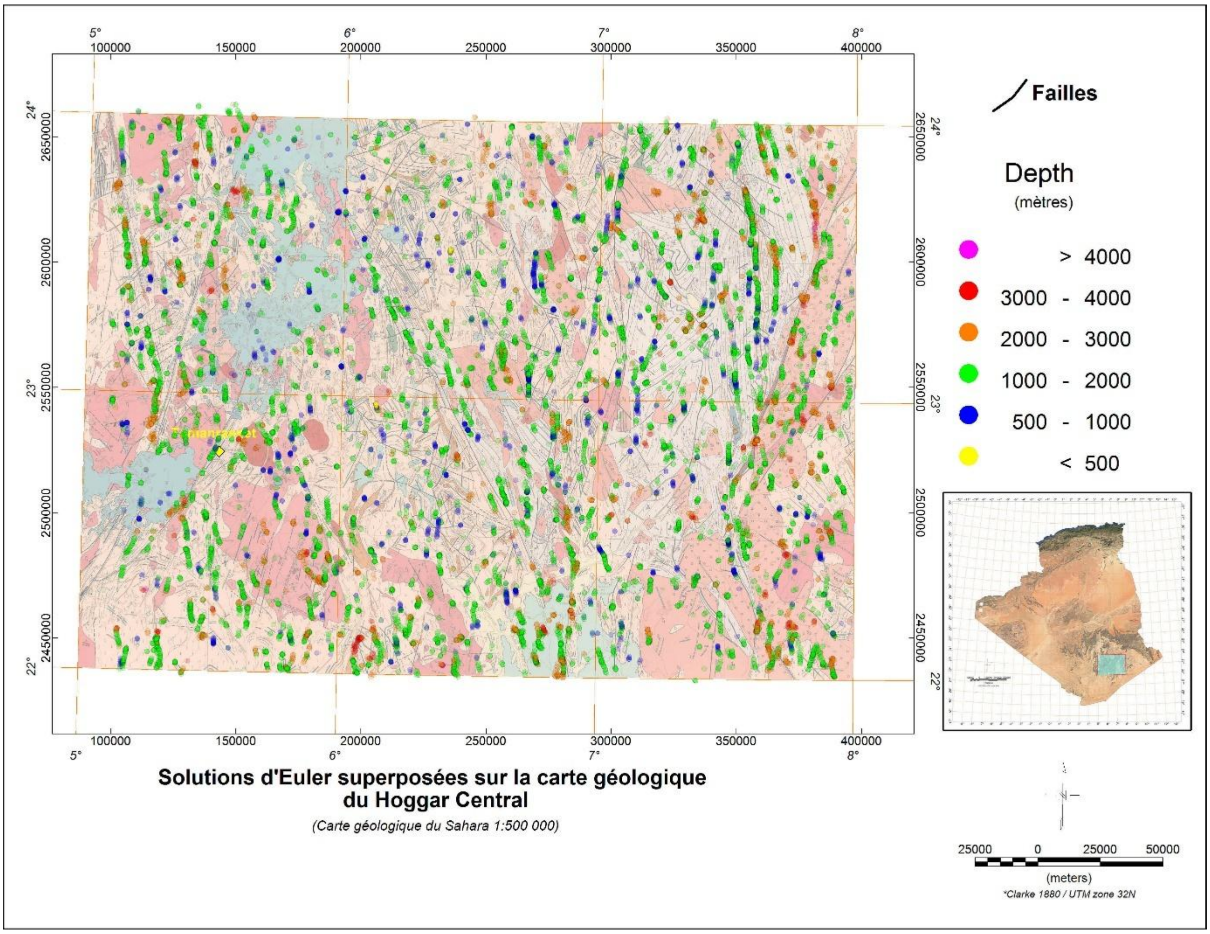

Fig 4.6 Euler solutions superimposed on the geological map of the Central Hoggar

CONCLUSION

In conclusion, this study successfully investigated the complex subsurface fault systems within the Latia region, located in the central Hoggar of southern Algeria, by leveraging inverse modeling and advanced processing techniques applied to aerial geophysical data. Through this integrated approach, we mapping and characterized the region's principal structural discontinuities, precisely identifying their spatial orientation, depth extent, lineament density, and associated secondary fault networks.

The definitive findings of this research can be synthesized into the following key points:

Efficacy of Data Optimization: While the raw aeromagnetic measurements demonstrated an acceptable initial quality, the rigorous application of geophysical corrections, filtering, and inverse mathematical methods proved essential. These processing steps significantly enhanced the signal-to-noise ratio, corrected for regional magnetic variations, and ensured precise structural repositioning, ultimately maximizing the visual clarity and definition of deeply buried geological structures.

Structural Architecture & Tectonics: Data processing and structural inversion revealed the presence of three major fault systems cutting through the Latia terrain. These primary structural trends correspond directly to the major pan-African orogenic features and subsequent tectonic reactivation events that shaped the central Hoggar shield. Furthermore, a network of secondary fault systems—exhibiting less spatial extent but carrying critical tectonic relevance—was successfully mapped, mapping out a highly fractured crystalline basement.

Ultimately, the results obtained from this structural inversion workflow contribute effectively to expanding exploration prospects for subsurface natural resources (such as hydroacoustic networks or mineralized vein systems) and serve as a robust, updated geophysical reference for future mapping of the geological infrastructure in the central Hoggar region

References

Chapter I: Geological Context

Allègre, C.J., and Caby, R. (1972). Chronologie absolue du Précambrien de l'Ahaggar occidental. Comptes Rendus de l'Académie des Sciences Paris, 275, 2095–2098.
Bertrand, J.M. (1974). Structures et évolution du Précambrien supérieur central du Hoggar (Algérie). Thèse de Doctorat, Université de Montpellier.
Bertrand, J.M., Michard, A., Boullier, A.M., and Dautel, D. (1978). Structure and geochronology of Central Hoggar (Algeria): A reappraisal. Canadian Journal of Earth Sciences, 23, 1472–1485.
Black, R., Latouche, L., Liégeois, J.P., Caby, R., and Bertrand, J.M. (1994). Pan-African displaced terranes in the Tuareg shield (central Sahara). Geology, 22, 641–644.
Caby, R. (1970). La chaîne pharusienne dans le Nord-Ouest de l'Ahaggar (Sahara central, Algérie): sa place dans l'orogenèse pan-africaine. Thèse, Université de Montpellier.
Caby, R. (2003). Terrane assembly and geodynamic evolution of central–western Hoggar: a synthesis. Journal of African Earth Sciences, 37, 133–159.
Caby, R., and Andreopoulos-Renaud, U. (1987). Age U-Pb sur zircons des leucogranites syntectoniques dans la chaîne pan-africaine de l'Adrar des Iforas (Mali). Precambrian Research, 36, 235–244.
Caby, R., Bertrand, J.M., and Black, R. (1981). Pan-African ocean closure and continental collision in the Hoggar–Iforas segment, central Sahara. In: A. Kroner (ed.), Precambrian Plate Tectonics. Elsevier, Amsterdam, 407–434.
Caby, R., Bertrand, J.M., Moussine-Pouchkine, A., and Sougy, J. (1982). The Pan-African orogeny in the Iforas massif. Bulletin de la Société géologique de France, 24, 851–860.
Caby, R., Andreopoulos-Renaud, U., and Pin, C. (2001). Late Proterozoic arc magmatism and continental accretion in the Tuareg shield. Precambrian Research, 108, 79–99.
Gravelle, M. (1969). Recherches sur la géologie du socle précambrien de la zone centrale de l'Ahaggar (Sahara central). CNRS, Paris.
Haddoum, H., Windley, B.F., Demaiffe, D., Liegeois, J.P., and Berriane, M. (1994). Pan-African granulites and associated high-pressure metamorphism in the In Ouzzal terrane (Hoggar, Algeria). Journal of African Earth Sciences, 18, 175–186.
Liégeois, J.P., Black, R., Navez, J., and Latouche, L. (1994). Early and late Pan-African orogenies in the Aïr assembly of terranes (Tuareg shield, Niger). Precambrian Research, 67, 59–88.
Liégeois, J.P., Latouche, L., Boughrara, M., Navez, J., and Guiraud, M. (2003). The LATEA metacraton (Central Hoggar, Tuareg shield, Algeria): behaviour of an old passive margin during the Pan-African orogeny. Journal of African Earth Sciences, 37, 161–190.

Chapter II: Geomagnetic Method

Blakely, R.J. (1995). Potential Theory in Gravity and Magnetic Applications. Cambridge University Press, Cambridge.
Chouteau, M. (1999). Méthodes électromagnétiques. Notes de cours, École Polytechnique de Montréal.
Dubois, J. (2011). Variations séculaires du champ géomagnétique. Institut de Physique du Globe de Paris.
Giroux, B., and Chouteau, M. (2011). Géophysique appliquée. Cours magistraux, École Polytechnique de Montréal.
Le Mouël, J.L. (1969). Sur la distribution des éléments magnétiques en France. Thèse de

Doctorat, Paris.
Telford, W.M., Geldart, L.P., and Sheriff, R.E. (1998). Applied Geophysics (2nd ed.). Cambridge University Press, Cambridge.

Chapter III: Description and Processing of Aerogeophysical Surveys

Aeroservice Corporation (1975). Rapport final du levé aéromagnétique de l'Algérie. Rapport interne, Direction de la Géologie, Algérie.
Baranov, V. (1957). A new method for interpretation of aeromagnetic maps: pseudo-gravimetric anomalies. Geophysics, 22, 359–383.
Baranov, V., and Naudy, H. (1964). Numerical calculation of the formula of reduction to the magnetic pole. Geophysics, 29, 67–79.
Bhattacharyya, B.K. (1965). Two-dimensional harmonic analysis as a tool for magnetic interpretation. Geophysics, 30, 829–857.
Blakely, R.J. (1995). Potential Theory in Gravity and Magnetic Applications. Cambridge University Press, Cambridge.
Gunn, P.J. (1975). Linear transformations of gravity and magnetic fields. Geophysical Prospecting, 23, 300–312.
Le Mouël, J.L. (1969). Sur la distribution des éléments magnétiques en France. Thèse de Doctorat, Paris.

Chapter IV: Interpretation of Aeromagnetic Data

Allek, K. (2005). Application des méthodes inverses à l'interprétation des données aéromagnétiques de la région de l'Ahaggar. Thèse de Magister, Université de Houari Boumediene, Alger.
Barboza, S.A., Bergantz, G.W., and Brown, M. (1999). Regional granulite facies metamorphism in the Ivrea zone: Is the metapelitic sequence a relic of a crustal-scale magmatic arc? Geology, 27, 1059–1062.
Blakely, R.J. (1995). Potential Theory in Gravity and Magnetic Applications. Cambridge University Press, Cambridge.
Gasquet, C., and Witomski, P. (1995). Analyse de Fourier et applications. Masson, Paris.
Groune, D. (2009). Traitement et interprétation des données géophysiques du Hoggar central. Rapport CRND, Draria, Alger.
Jacobsen, B.H. (1987). A case for upward continuation as a standard separation filter for potential-field maps. Geophysics, 52, 1138–1148.
Keating, P.B. (1998). Euler deconvolution of the analytical signal. Geophysics, 63, 1932–1936.
Mushayandebvu, M.F., van Driel, P., Reid, A.B., and Fairhead, J.D. (2001). Magnetic source parameters of two-dimensional structures using extended Euler deconvolution. Geophysics, 66, 814–823.
Nabighian, M.N. (1972). The analytic signal of two-dimensional magnetic bodies with polygonal cross-section: its properties and use for automated anomaly interpretation. Geophysics, 37, 507–517.
Nabighian, M.N. (1974). Additional comments on the analytic signal of two-dimensional magnetic bodies with polygonal cross-section. Geophysics, 39, 85–92.
Nabighian, M.N. (1984). Toward a three-dimensional automatic interpretation of potential field data via generalized Hilbert transforms: fundamental relations. Geophysics, 49, 957–966.
Reid, A.B., Allsop, J.M., Granser, H., Millett, A.J., and Somerton, I.W. (1990). Magnetic

interpretation in three dimensions using Euler deconvolution. Geophysics, 55, 80–91.
Roest, W.R., Verhoef, J., and Pilkington, M. (1992). Magnetic interpretation using the 3-D analytic signal. Geophysics, 57, 116–125.
Silva, J.B.C., and Barbosa, V.C.F. (2003). 3D Euler deconvolution: Theoretical basis for automatically selecting good solutions. Geophysics, 68, 1962–1968.
Silva, J.B.C., Medeiros, W.E., and Barbosa, V.C.F. (2001). Potential-field inversion: Choosing the appropriate technique to solve a geologic problem. Geophysics, 66, 511–520.